J. Fluid Mech. (1991), *vol.* 222, *pp.* 1–32
Printed in Great Britain

The influence of surfactant adsorption on the motion of a fluid sphere in a tube. Part 1. Uniform retardation controlled by sorption kinetics

By ZUNQING HE[1], ZEEV DAGAN[2] AND CHARLES MALDARELLI[1]†

[1] Levich Institute for Physicochemical Hydrodynamics, Department of Chemical Engineering, City College of New York, New York, NY 10031, USA

[2] Department of Mechanical Engineering, City College of New York, New York, NY 10031, USA

(Received 30 November 1988 and in revised form 30 April 1990)

This paper presents a study of the steady, axisymmetric, creeping translation of a fluid sphere in a tube for the case in which surfactant is adsorbed onto the fluid sphere interface. Marangoni stresses caused by the convective redistribution of surfactant are computed perturbatively in the limit of sorption-controlled uniform retardation, and fully converged numerical solutions of the creeping-flow equations including the Marangoni stress are obtained by a collocation technique.

The results indicate that when the fluid sphere moves in a liquid which is at rest at infinity, the Marangoni stress retards the particle velocity. This retardation generally increases with the sphere to tube diameter ratio up to a value of approximately 0.6, whereupon the retardation begins to level off or even become reduced. When the sphere is suspended in a Poiseuille flow, stagnation rings develop on the sphere surface, and the Marangoni stresses that derive from this surface convection pattern can accelerate the fluid particle when the particle velocity is small with respect to the Poiseuille centreline velocity, but in the same direction as that velocity.

1. Introduction

This study is the first of a two-part theoretical examination of the steady, axisymmetric, creeping translation of a fluid sphere in a tube for the case in which bulk-soluble surface-active molecules are adsorbed onto the sphere interface. The general mechanism by which surfactant adsorption onto fluid interfaces affects the interface hydrodynamics was first formulated by Frumkin & Levich (1947). Surfactant molecules which kinetically adsorb onto a clean fluid interface are swept to stagnation regions on the surface where the interfacial flow converges. At these regions the surfactant molecules may accumulate, or kinetically desorb and subsequently diffuse away from the particle vicinity. Surfactant accumulation at a converging stagnation region of the fluid surface locally lowers the interfacial tension relative to the neighbouring area. The interface is therefore tugged in a direction away from the stagnation region, and towards the bordering regions of lower surface concentration and higher interfacial tension. The consequences of this Marangoni

† Author to whom correspondence should be addressed.

stress are twofold. First, as it is directed opposite to that of the surface flow, it retards the interface velocity. Second, at steady state, the Marangoni tension is balanced by a viscous traction exerted on the surface by the adjoining phases. In the case of the movement of fluid particles, this traction changes the drag exerted on the particle by the continuous phase as compared to the clean-surface value.

When the fluid particle translates in an infinite medium, the effect of the Marangoni stress is straightforward. The surface flow pattern is unidirectional, emerging from the leading stagnation pole and converging at the trailing one. Surfactant is convected to the rear pole, creating a Marangoni tension which is exerted away from the rear. This tension reduces the surface velocity. The Marangoni tension is also balanced by an opposing viscous traction which retards the fluid particle velocity since it acts in a direction opposite to the direction of motion of the particle. The infinite-medium problem of the movement of a fluid sphere has been the subject of many theoretical studies which have explored the regimes of slow kinetic or diffusive exchange between the bulk and the surface (stagnant-cap behaviour, see Savic 1953; Davis & Acrivos 1966; Sadhal & Johnson 1982), fast exchange (uniform retardation, see Levich 1962; Schechter & Farley 1963; Newman 1967), and finite-diffusion-limited or sorption-kinetic-limited exchange (Wasserman & Slattery 1969; Harper 1973, 1982; Saville 1973; Levan & Newman 1976; Holbrook & Levan 1983*a*, *b*; Levan & Holbrook 1989).

When a fluid particle translates in a tube, the surface flow pattern can become more complicated, and discerning the partitioning of surfactant on the surface, and calculating the Marangoni tension, is a correspondingly more difficult task. If the particle moves by virtue only of a body force, and the fluid at infinity is at rest, then in a reference frame fixed to the particle, the surface flow is from the leading to the trailing pole. This is the case of uniform flow at infinity and it is analogous to that of the movement of a fluid particle in an infinite medium: surfactant is convected to the rear pole and the viscous traction which balances the Marangoni tension reduces the particle velocity. For this case of uniform flow at infinity, the feature that distinguishes motion in a tube from an infinite medium is that for the same particle velocity, the surface convection is stronger in the tube flow because of the presence of the wall boundary. The accumulation of surfactant at the trailing pole is proportionately higher, and hence so is the retarding drag.

If the fluid particle is suspended in a Poiseuille flow, then, in a particle fixed frame, two stagnation rings can develop on the particle surface if the particle velocity is less than (but in the same direction as) the centreline velocity of the suspending flow. When stagnation rings develop, fluid diverges from the front ring and back pole, and converges to the trailing ring and front pole. Hence surfactant is swept towards the front pole and the back ring. The accumulation caused by convection towards the front pole, and from the back pole to the back ring, gives rise to Marangoni tensions which can increase the particle velocity, although these will be modulated by the tension set up by accumulation from the flow from the front ring to the back ring.

The aim of the present paper and Part 2 (He, Dagan & Maldarelli 1990) is (i) to quantify the hydrodynamic interaction of the tube wall with the surface of a surfactant-laden fluid particle for the case in which the particle moves in a liquid at rest, and (ii) to understand whether the particle velocity is retarded or accelerated when it is suspended in a Poiseuille flow and stagnation rings develop. These papers will only examine the case of single fluid *spheres* moving axisymmetrically and at low Reynolds number through the cylindrical tube, and will focus on the computation of the hydrodynamic drag exerted by the continuous phase on the sphere. Studies of the

axisymmetric, low-Reynolds-number translation of surfactant-laden fluid spheres in tubes are not available in the literature, although the underlying clean surface flow has been examined both approximately for small to moderate sphere to tube diameter ratios (Haberman & Sayre 1985; Brenner 1970, 1971), and exactly by numerical solution (Hyman & Skalak 1969, 1970).

The consideration of fluid spheres in these two papers leaves unresolved the effect of surfactants on the movement of non-spherical particles in tubes, most notably fluid slugs. Again, the clean flow problem is well understood both asymptotically and numerically (Bretherton 1961; Park & Homsy 1984; Shen & Udell 1985; Reinelt & Saffman 1985; Westborg & Hassager 1989; Martinez & Udell 1989, 1990). However, the influence of surfactants on the movement of a fluid slug is only beginning to be theoretically studied (cf. the work of Bretherton 1961 and Goldsmith & Mason 1973 which assume a rigid interface in the bubble-fixed frame – this model is also discussed in the text by Probstein 1989, Hirasaki & Lawson 1985, Moulai-Mostefa, Meister & Barthes-Bissel 1986 and Ginley & Radke 1989 on the regime of uniform retardation controlled by sorption kinetics, Herbolzheimer 1987 for a regime in which the surface velocity is zero in the laboratory-fixed frame, and Ratulowski & Chang 1990 for a discussion of the effects of finite diffusive and kinetic exchange in the limit of an asymptotically small bulk concentration of surfactant). The intention here is that the results obtained in these two papers on fluid spheres, especially those concerning the hydrodynamic drag and the surfactant partitioning when two stagnation rings are present on the interface, should prove useful to the study of the impact of surfactants on the slug flow regime.

In this first paper, it is assumed that the rate at which surfactant kinetically desorbs from the fluid sphere surface is fast in comparison to the rate at which it is transported along the surface by convection. Further, the rate of diffusive exchange between the bulk and the sublayer is assumed to be faster than the kinetic desorption process, and therefore the surfactant distribution is only controlled by the desorption step. For this regime, because the desorption and diffusive transport processes are fast, surfactant cannot accumulate at converging surface stagnation points, and the surface concentration only deviates slightly from the uniform value achieved with no flow. Since the uniform distribution does not create a Marangoni stress, drag coefficients are determined as perturbative corrections to the clean surface case. The second part of this series (He *et al.* 1990) studies the opposite regime in which the surfactant desorption kinetics is slower than surface convection (and the sublayer–surface diffusive exchange), and a stagnant cap whose size is determined by the desorption step develops in the region of accumulation.

In each of these papers, exact numerical solutions of the steady creeping-flow equations are obtained by a method first outlined by Leichtberg, Pfeffer & Weinbaum (1976) in the study of the motion of clusters of solid spheres in tubes: general analytical solutions of the stream-function equations for flow in the fluid space between the particle and the tube wall that satisfy exactly the wall kinematic constraints are constructed, and then the conditions on the sphere surface are satisfied by collocation.

This paper is organized into five sections. Section 2 details the exact governing equations and boundary conditions (§2.1), and outlines the perturbation scheme that describes the regime of kinetically controlled uniform retardation (§2.2). Section 3 outlines the numerical solution procedure. The solution technique involves exact satisfaction of the wall hydrodynamic conditions, and a pointwise satisfaction of the kinematic and surfactant mass transfer conditions at the spherical particle interface

(§3.1). Convergence criteria and a verification of the method by comparison to the results for solid spheres and fluid spheres uncontaminated with adsorbed surfactant are presented in §3.2. The results, detailed in §4, consist of the tabulations of hydrodynamic drag coefficients (§4.1), and the calculation of terminal velocities and the presentation of velocity fields (§4.2) for several flow regimes. The paper ends with conclusions (§5).

2. Formulation

2.1. *Governing equations and boundary conditions*

The problem under examination is that of a fluid droplet moving steadily and axisymmetrically through a continuous liquid in an infinitely long cylindrical tube. Both the droplet and continuous phases are assumed to be incompressible and Newtonian. Far away from the droplet, the continuous fluid flow is either stationary or Poiseuillian. The Reynolds and capillary numbers are assumed to be small enough that inertia is negligible and the droplet retains a spherical shape. A bulk-soluble surfactant is present in the continuous phase and is adsorbed on the surface of the droplet. The concentration of surfactant far from the droplet is assumed to be uniform. In the solution technique that will be used both cylindrical (ρ, ω, z) and spherical coordinates (r, θ, ϕ) are needed. The origin of both systems is located at the centre of the moving droplet, and therefore in these systems the tube wall is moving in the axial direction (see figure 1). The velocity of the droplet in the absence of the surfactants is denoted as U_0'. (Dimensional quantities are marked by a prime, and dimensionless quantities are unprimed throughout the analysis.) U_0' is taken as positive when the drop is moving in the positive z-direction, and therefore, in the droplet frame, the wall is moving in the $-z$-direction when U_0' is greater than zero. The centreline velocity in the Poiseuille flow is denoted as V' and is taken as positive when Poiseuille flow is in the $+z$-direction. The angle θ is measured from the front stagnant point and the gravitational force is acting in the $-z$-direction.

In formulating the hydrodynamic equations for the droplet motion, droplet and continuous-phase variables are denoted by superscripts (1) and (2) respectively. The tube and the droplet radius are denoted by b' and a' respectively. Coordinates are non-dimensionalized by the droplet radius a'. The kinematic variables (of both phases) are scaled as follows: velocities by the steady translational velocity of the droplet in the absence of the surfactant in the tube, U_0', and shear stress tensors τ_{ij}' and pressure P' by $\mu'^{(2)}U_0'/a'$, where $\mu'^{(2)}$ is the viscosity of the exterior fluid. The ratio of the droplet to continuous-phase viscosity is denoted by $\kappa\,(\kappa = \mu'^{(1)}/\mu'^{(2)})$. The surfactant concentration Γ' is non-dimensionalized by Γ_0', which is the surfactant concentration in equilibrium with the uniform bulk concentration C_∞'. The bulk concentration C' in the continuous phase is non-dimensionalized by the far-field value C_∞'. Since the flow is axisymmetric and incompressible, velocities may be represented by a stream function ψ', which is non-dimensionalized by $a'^{(2)}U_0'$.

The Navier–Stokes equation for axisymmetric flow can be written in terms of a stream function $\psi^{(i)}$ (Happel & Brenner 1973). This stream function can be expressed in terms of cylindrical (ρ, z) or spherical (r, θ) coordinates. For the drop phase, only the representation in spherical coordinates is necessary, and is denoted $\psi_{(s)}^{(1)}(r, \theta)$, while for the exterior phase, equivalent representations for the stream function in terms of either cylindrical $(\psi_{(c)}^{(2)}(z, \rho))$ or spherical $(\psi_{(s)}^{(2)}(r, \theta))$ coordinates proves useful. (Note that the two representations are related through the coordinate transformation; thus $\psi_{(s)}^{(2)}(r, \theta) = \psi_{(c)}^{(2)}(\rho = r\sin\theta, z = r\cos\theta)$.) When ψ is expressed in

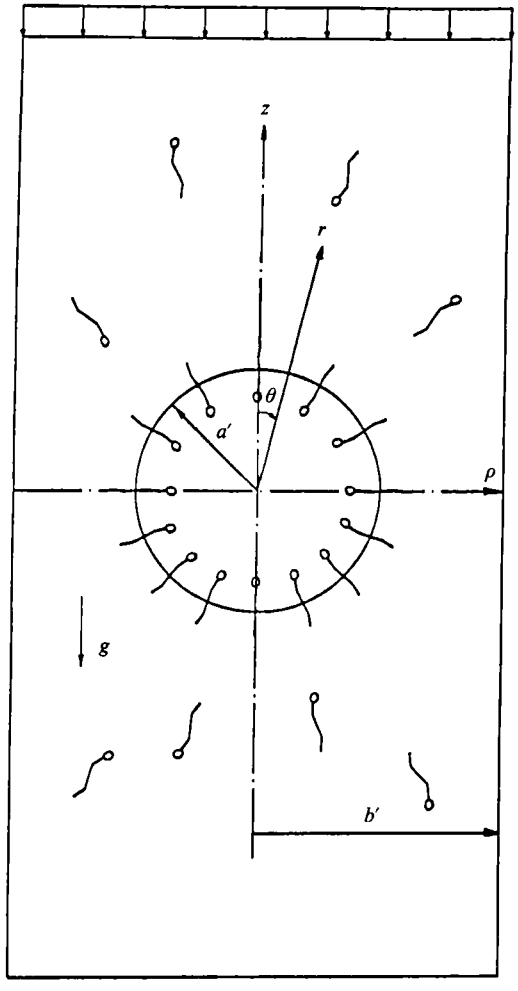

FIGURE 1. Definition sketch of the axisymmetric motion in a tube in a frame moving with the spherical fluid particle velocity. The sketch presents the case for motion in an otherwise quiescent medium; for suspension in Poiseuille flow the flow at infinity would be a parabolic profile added to the uniform flow. The presence of surfactants in the continuous phase is indicated by the figures with heads and tails.

spherical coordinates, the stream function satisfies the equation $E^2_{(s)}(E^2_{(s)}\,\psi^{(i)}_{(s)}) = 0$, where

$$E^2_{(s)}\,\psi^{(i)}_{(s)} = \frac{\partial^2\psi^{(i)}_s}{\partial r^2} + \frac{\sin\theta}{r^2}\frac{\partial}{\partial\theta}\left(\frac{1}{\sin\theta}\frac{\partial\psi^{(i)}_s}{\partial\theta}\right), \tag{2.1}$$

and the velocity components are given by

$$V^{(i)}_{(s)\,r} = -\frac{1}{r^2\sin\theta}\frac{\partial\psi^{(i)}_s}{\partial\theta}, \quad V^{(i)}_{(s)\,\theta} = \frac{1}{r\sin\theta}\frac{\partial\psi^{(i)}_s}{\partial r}. \tag{2.2}$$

In the above, the subscript 's' denotes the spherical representation of the velocity vector field. When expressed in cylindrical coordinates, the stream function satisfies the equation $E^2_{(c)}(E^2_{(c)}\,\psi^{(i)}_{(c)}) = 0$, where

$$E^2_{(c)}\,\psi^{(i)} = \frac{\partial^2\psi^{(i)}_{(c)}}{\partial z^2} + \frac{\partial^2\psi^{(i)}_c}{\partial\rho^2} - \frac{1}{\rho}\frac{\partial\psi^{(i)}_c}{\partial\rho}, \tag{2.3}$$

and the velocity components are given by

$$V^{(i)}_{(c)z} = -\frac{1}{\rho}\frac{\partial \psi^{(i)}_c}{\partial \rho}, \quad V^{(i)}_{(c)\rho} = \frac{1}{\rho}\frac{\partial \psi^{(i)}_c}{\partial z}. \tag{2.4}$$

The boundary conditions are formulated at the centre of the droplet, the tube wall, the droplet surface and far from the droplet. These are:

(i) At the droplet centre, $\lim_{r\to 0} V^{(1)}_{(s)r}$ and $\lim_{r\to 0} V^{(1)}_{(s)\theta}$ exist.

(ii) Far from the droplet, the velocity field is either uniform

$$\lim_{|z|\to\infty} V^{(2)}_{(c)z} = -U \tag{2.5}$$

or of Poiseuille type

$$\lim_{|z|\to\infty} V^{(2)}_{(c)z} = V\left(1-\frac{\rho^2}{b^2}\right)-U, \tag{2.6}$$

where U is the velocity of the droplet and V is the centreline velocity of the Poiseuille flow at infinity (non-dimensionalized by U'_0).

(iii) At the tube wall, $\rho = b\,(b = b'/a')$

$$V^{(2)}_{(c)z} = -U, \quad V^{(2)}_{(c)\rho} = 0. \tag{2.7}$$

(iv) At the surface of the droplet, $r = 1\,(r = r'/a' = 1)$

$$V^{(1)}_{(s)r} = V^{(2)}_{(s)r} = 0, \tag{2.8}$$

$$V^{(1)}_{(s)\theta} = V^{(2)}_{(s)\theta}, \tag{2.9}$$

$$\tau^{(2)}_{(s)r\theta} - \tau^{(1)}_{(s)r\theta} + \frac{1}{\mu'^{(2)}U'_0}\frac{\partial \sigma'}{\partial \Gamma'}\frac{\partial \Gamma'}{\partial \theta} = 0, \tag{2.10}$$

where σ' is the surface tension, and the last term on the left-hand side of (2.10) represents the Marangoni stress due to the surfactant gradient.

Owing to the assumption that the droplet retains its spherical shape, the normal stress balance on the interface is replaced by an integrated force balance:

$$F'_z = 2\pi\mu'^{(2)}U'_0 a' \int_0^\pi \{(-P^{(2)}_{(s)} + \tau^{(2)}_{(s)rr})\cos\theta - \tau^{(2)}_{(s)r\theta}\sin\theta\}\sin\theta\,\mathrm{d}\theta$$

$$= \tfrac{4}{3}\pi a'^3(\rho'^{(1)} - \rho'^{(2)})\,g', \tag{2.11a}$$

where F'_z is the hydrodynamic drag exerted by the exterior fluid on the drop, $\rho'^{(i)}$ is the density of phase i and g' is the gravitational acceleration. Equation (2.11a) will be used to determine the droplet terminal velocities. Writing the normal ($\tau^{(2)}_{(s)rr}$) and shear ($\tau^{(2)}_{(s)r\theta}$) stresses in terms of the stream function, (2.11a) may be expressed in the form

$$F'_z = a'U'_0\mu'^{(2)}\pi \int_0^\pi r^4 \sin^3\theta \frac{\partial}{\partial r}\left[\frac{E^2\psi^{(2)}_s}{r^2\sin^2\theta}\right]\mathrm{d}\theta, \tag{2.11b}$$

where after the differentiation the integrand is evaluated at $r = 1$.

To evaluate the Marangoni stress term in (2.10), the surfactant concentration $\Gamma'(\theta)$ must be determined. This concentration is obtained from the solution of the

equations of surfactant conservation at the interface of the droplet and in the surrounding bulk phase. To formulate the interfacial conservation balance, Langmuir kinetics is used to describe the adsorptive and desorptive exchange of surfactant molecules between the surface and the bulk sublayer adjacent to the interface. Thus the sublayer–surface exchange, Q', is given dimensionally by $Q' = -\alpha'\Gamma' - \beta' C'_{(s)}(r = 1, \theta)(\Gamma' - \Gamma'_\infty)$, where α' and β' are kinetic constants of desorption and adsorption respectively, $C'_{(s)}(r = 1, \theta)$ is the sublayer concentration and Γ'_∞ is the limiting surface concentration. (Note that the subscript (s) which appears with C identifies the spherical coordinate representation of the concentration field.) The surface concentration which is in equilibrium with C'_∞ is obtained from the condition $Q' = 0$, and is given by $\Gamma'_0/\Gamma'_\infty = k/(1+k)$, where Γ'_0 denotes the equilibrium surface coverage and $k = \beta' C'_\infty/\alpha'$. Note that k represents the ratio of the rates of adsorption and desorption.

Using Langmuir kinetics, the non-dimensional form for the interfacial mass balance becomes:

$$\frac{1}{\sin\theta}\frac{\partial}{\partial\theta}(\sin\theta\,\Gamma V_{(s)\theta}(r=1,\theta)) = \frac{1}{Pe_s \sin\theta}\frac{\partial}{\partial\theta}\left(\sin\theta\frac{\partial\Gamma}{\partial\theta}\right) - \nu[C_{(s)}(r=1,\theta)\,k(\Gamma - 1 - 1/k) + \Gamma], \quad (2.12)$$

where Γ represents the surface concentration non-dimensionalized with Γ'_0 and Pe_s is the surface Péclet number ($Pe_s = a'U'_0/D'_s$, D'_s is the surface diffusion coefficient). The parameter ν appearing in (2.12) is given by $\nu = \alpha'/(U'_0/a')$, and represents the non-dimensional ratio of the rate of desorption of surfactant off the surface to the rate at which surfactant is convected from one end of the droplet to the other. Note finally that with the choice of Langmuir kinetics, the equilibrium relation for $\sigma'(\Gamma')$, which follows from the Gibbs adsorption relation, is given by the Frumkin equation $\sigma' = \sigma'_0 - R'T'\Gamma'_\infty \ln(1/(1-\Gamma'/\Gamma'_\infty))$, where σ'_0 is the surface tension of the clean interface. Consequently, $\partial\sigma'/\partial\Gamma'$ appearing in the tangential stress condition is calculated to be

$$\frac{\partial\sigma'}{\partial\Gamma'} = -\frac{R'T'}{(1-\Gamma'/\Gamma'_\infty)}. \quad (2.13)$$

The sublayer concentration is obtained from the solution of the bulk convective–diffusion equation for the surfactant transport:

$$Pe\boldsymbol{V}\cdot\boldsymbol{\nabla}C = \nabla^2 C, \quad (2.14)$$

where ∇^2 is the Laplacian operator, $Pe = U'_0 a'/D'$, D' is the bulk diffusivity of the surfactant and C is the bulk concentration. The boundary conditions on the bulk concentration are

$$\Phi(1+k)\left.\frac{\partial C_{(s)}}{\partial r}\right|_{r=1} = \nu\left[kC_{(s)}(r=1,\theta)\left(\Gamma - 1 - \frac{1}{k}\right) + \Gamma\right] \quad (2.15)$$

and

$$\lim_{|z|\to\infty} C_{(c)}(z,\rho) = 1, \quad (2.16)$$

$$\left.\frac{\partial C_{(c)}}{\partial\rho}\right|_{\rho=b} = 0. \quad (2.17)$$

In (2.15), $\Phi = D'\alpha'/(\beta' U'_0 \Gamma'_\infty)$, and $\Phi(1+k)$ can easily be shown to be equal to

$Pe^{-1}(a'/h')$, where h' is the adsorption depth of the surfactant and is equal to Γ_0'/C_∞'. The adsorption depth is the depth beneath the surface which contains (per unit area) as much surfactant as that on the surface at equilibrium. This completes the formulation.

2.2. *Uniform retardation perturbation scheme*

As remarked in the Introduction, this study examines the regime in which (i) both the desorptive kinetic exchange between the surface and the sublayer, and the diffusive exchange between the bulk and the sublayer, are fast in relation to surface convection, and (ii) the bulk diffusive exchange is faster than that of the desorptive kinetics so that the desorption process is rate controlling. For this range of parameters, the surface concentration of surfactant only deviates slightly from the uniform equilibrium value, and the steady drop velocity is only perturbatively affected from the clean surface value. Uniform retardation controlled by desorption kinetics is described in terms of the non-dimensional groups introduced in §2.1 by the inequalities: (i) $\nu \gg 1$ (rate of desorption fast when compared to the rate of surface convection), and (ii) $\Phi(1+k) \gg \nu$ (diffusive exchange fast when compared to desorption). It should be noted that to achieve this uniformally retarded regime, the rate of adsorption relative to that of desorption (as measured by the parameter k) is not crucial. The perturbation analysis to follow will more precisely define the role of k (cf. §3.2), but it is noted here that: (i) if $k \to 0$ (rate of desorption rate faster than that of adsorption), the first-order perturbation in the droplet velocity equals zero since the amount of surfactant adsorbed onto the surface becomes zero, and (ii) if $k \to \infty$ (adsorption much faster than desorption), uniform retardation is still realized, and the largest affect on the drop velocity is achieved since the largest amount of surfactant is adsorbed onto the surface.

The above inequalities necessary for desorption-controlled uniform retardation ($\nu \gg 1$; $\Phi(1+k) \gg \nu$) are not too restrictive: for example, they appear to be suitable for the important case (from the standpoint of tertiary oil recovery) of the movement of drops in micron-sized channels of rock pores as long as the translational velocity U_0' and the adsorption depth h' are sufficiently small. Consider, for example, pore diameters of the order of 1 μm, fluid spheres of approximately the same size and alcohols as the surface-active species. For the straight-chain n-alcohols, adsorption depths near the miscibility limit are (for $n < 8$) of the order of 0.1 μm or less (see for example Hommelen 1959), and unsteady tensiomctry experiments by Bleys & Joos (1985) and Joos & Serrien (1989) indicate that α' is of the order of 10^2 s^{-1} for these alcohols. Therefore in order for the convective rate to be less than the desorptive rate, $U_0' < 10^{-3}$ cm/s. The second condition, $\Phi(1+k) \gg \nu$ or $Pe^{-1}(a'/h') \gg \nu$, is also satisfied for D of the order of 10^{-6} cm^2 s^{-1} as long as h is of the order of 10^{-1} μm or smaller. Thus, for a fixed diameter and desorption rate constant, the restriction that the bulk diffusion is fast when compared to the desorption is satisfied by requiring a sufficiently small adsorption depth (or a large enough bulk concentration), and the restriction that the desorption is fast when compared to the surface convection is satisfied by requiring a sufficiently slow particle movement.

One further point should be addresed with regard to realizing this uniformally retarded regime: the desorption rate must be of the same order as or larger than the surface diffusion rate (i.e. $\nu \geqslant 1/Pe_s$ or $\alpha' a'^2/D_s' \geqslant 1$). For the case cited above, this condition is satisfied with D_s' of the order of 10^{-6}–10^{-7} cm^2/s (one order of magnitude smaller than the bulk diffusivity).

To describe the regime of uniform retardation controlled by desorption kinetics in a precise, asymptotic manner, ν is scaled to order ϵ^{-1} ($\nu = \nu^*/\epsilon$), $(\nu/(Pe^{-1}(a'/h'))) =$

$O(\epsilon)$, and $(Pe_s\nu)^{-1} = O(1)$ (or $O(\epsilon)$; it is not important to the first non-trivial order). The stream function, terminal velocity and surface and bulk concentration of surfactant are expanded in asymptotic series in powers of ϵ as follows:

$$\left.\begin{aligned} \psi &= \psi_{(0)} + \epsilon\psi_{(1)} + O(\epsilon^2), \\ U &= U_{(0)} + \epsilon U_{(1)} +)(\epsilon^2), \\ \Gamma &= \Gamma_{(0)} + \epsilon\Gamma_{(1)} + O(\epsilon^2), \\ C &= C_{(0)} + \epsilon C_{(1)} + O(\epsilon^2), \end{aligned}\right\} \tag{2.18}$$

where the subscripts indicate the asymptotic order of the variables. Attention in this study will be confined to the zeroth- and first-order variables.

For the zeroth order, the diffusive uptake of surfactant (2.15) is equal to zero, and it can therefore easily be concluded from the zeroth orders of (2.14), (2.16) and (2.17) that $C_{(0)} = 1$. Further, the surface kinetics is in equilibrium and therefore $\Gamma_{(0)} = 1$. The remainder of the zeroth-order equations become

$$E^2(E^2\psi^{(f)}_{(0)}) = 0, \tag{2.19}$$

$$\left.\begin{aligned} \lim_{|z|\to\infty} V^{(2)}_{(c)\,z(0)} &= -U_{(0)} \qquad \text{(uniform flow)}, \\ \lim_{|z|\to\infty} V^{(2)}_{(c)\,z(0)} &= V\left(1-\frac{\rho^2}{b^2}\right) - U_{(0)} \quad \text{(Poiseuille flow)}, \end{aligned}\right\} \tag{2.20}$$

$$V^{(2)}_{(c)\,z(0)} = -U_{(0)} \quad \text{and} \quad V^{(2)}_{(c)\,\rho(0)} = 0 \quad (\rho = b), \tag{2.21a, b}$$

$$V^{(1)}_{(s)\,r(0)} = V^{(2)}_{(s)\,r(0)} = 0 \quad \text{and} \quad V^{(1)}_{(s)\,\theta(0)} = V^{(2)}_{(s)\,\theta(0)} \quad (r = 1), \tag{2.22a, b, c}$$

$$\tau^{(2)}_{(s)\,r\theta(0)} - \tau^{(1)}_{(s)\,r\theta(0)} = 0 \quad (r = 1), \tag{2.23}$$

$$\int_0^\pi \{(-P^{(2)}_{(s)(0)} + \tau^{(2)}_{(s)\,r\theta(0)})\cos\theta - \tau^{(2)}_{(s)\,r\theta(0)}\sin\theta\}\sin\theta\,\mathrm{d}\theta = \frac{2a'^2(\rho'^{(1)} - \rho'^{(2)})g'}{3\mu'^{(2)}U'_0} \quad (r = 1). \tag{2.24}$$

Thus the zeroth-order solution is just the solution for the hydrodynamic field in the absence of surfactant, and $U_{(0)} = 1$.

For the first order, the diffusive uptake is once again zero, and it can easily be shown that this leads to $C_{(1)}$ being everywhere zero. The first-order surfactant balance becomes

$$\frac{1}{\sin\theta}\frac{\partial}{\partial\theta}(\sin\theta\, V_{(s)\,\theta(0)}(r = 1, \theta)) = -\nu^*(1+k)\,\Gamma_{(1)}. \tag{2.25}$$

This expression for $\Gamma_{(1)}$ can be combined with the first-order tangential balance to yield

$$\tau^{(2)}_{(s)\,r\theta(1)} - \tau^{(1)}_{(s)\,r\theta(1)} = -\phi\frac{\partial}{\partial\theta}\left(\frac{1}{\sin\theta}\frac{\partial}{\partial\theta}\sin\theta\, V_{(s)\,\theta(0)}(r = 1, \theta)\right) \quad (r = 1), \tag{2.26}$$

where

$$\phi = \frac{R'T'\Gamma'_\infty}{\mu'^{(2)}U'_0}\frac{k}{(1+k)\,\nu^*}.$$

The remainder of the first-order equations are summarized below:

$$E^2(E^2\psi^{(i)}_{(1)}) = 0, \tag{2.27}$$

$$\lim_{|z|\to\infty} V^{(2)}_{(c)\,z(1)} = -U_{(1)} \quad \text{(uniform or Poiseuille flow)}, \tag{2.28}$$

$$V^{(2)}_{(c)\,z(1)} = -U_{(1)} \quad \text{and} \quad V^{(2)}_{(c)\,\rho(1)} = 0 \quad (\rho = b), \tag{2.29a, b}$$

$$V^{(1)}_{(s)\,r(1)} = V^{(2)}_{(s)\,r(1)} = 0 \quad \text{and} \quad V^{(1)}_{(s)\,\theta(1)} = V^{(2)}_{(s)\,\theta(1)} \quad (r = 1), \tag{2.30a, b, c}$$

$$\int_0^\pi \{(-P^{(2)}_{(s)\,(1)} + \tau^{(2)}_{(s)\,rr(1)})\cos\theta - \tau^{(2)}_{(s)\,r\theta(1)}\sin\theta\}\sin\theta\,\mathrm{d}\theta = 0 \quad (r = 1). \tag{2.31}$$

Note that to first order the drag on the fluid sphere is equal to zero.

3. Solution technique

3.1. *Construction of field equation solutions and satisfaction of boundary conditions*

From the defining relations for the boundary-value problems of the zero and first order, it can easily be shown that the stream function for these orders is a symmetric function of z, i.e. $\psi_{(c)\,(i)}(\rho, z) = \psi_{(c)\,(i)}(\rho, -z)$ $(i = 1, 2)$. In view of (2.2) and the cylindrical–spherical transformation relations, the symmetry in $\psi_{(c)\,(0)}(\rho, z)$ requires that the zeroth-order surface velocity be symmetric with respect to z ($(V_{(s)\,\theta(0)}(r = 1, \theta)) = V_{(s)\,\theta(0)}(r = 1, \pi - \theta)$), and consequently from (2.26) the first-order surface concentration is antisymmetric in z ($\Gamma_{(1)}(\theta) = -\Gamma_{(1)}(\pi - \theta)$). By taking into account these reflectional properties, the computational effort is reduced considerably.

The solution of (2.1) or (2.3) may be obtained by the method of separation of variables. For the droplet interior, only the solution in spherical coordinates is needed. The form for $\psi^{(1)}_{(s)\,(i)}(r, \theta)$ that admits bounded solutions as $r \to 0$ for $V^{(1)}_{(s)\,r(i)}$ and $V^{(1)}_{(s)\,\theta(i)}$ (as given by (2.2) and that is symmetric in z is

$$\psi^{(1)}_{(s)\,(i)} = \sum_{n=2}^{\infty} (E^{(1)}_{n(i)}\, r^n + F^{(1)}_{n(i)}\, r^{n+2})\, C^{-\frac{1}{2}}_n(\cos\theta), \quad (n \text{ even}), \tag{3.1}$$

where $C^{-\frac{1}{2}}_n(\cos\theta)$ is the Gegenbauer polynomial of order n and degree $-\frac{1}{2}$.

For the continuous fluid, a sufficiently general solution is constructed in the following manner. The cylindrical-coordinate solution of (2.3) that is symmetric in z and that matches the far-field flow as $|z| \to \infty$ is of the form

$$\psi^{(2)}_{(c)\,(i)}(\rho, z) = \psi^{\infty}_{(c)\,(i)}(\rho) + \int_0^\infty \mathrm{d}k\{A_{(i)}(k)\,\rho I_1(k\rho) + B_{(i)}(k)\,\rho^2 I_0(k\rho)\}\cos(kz)$$
$$+ \int_0^\infty \mathrm{d}k\{C_{(i)}(k)\,\rho K_1(k\rho) + D_{(i)}(k)\,\rho^2 K_0(k\rho)\}\cos(kz), \tag{3.2}$$

where
$$\psi^{\infty}_{(c)\,(0)}(\rho) = \begin{cases} \frac{1}{2}\rho^2 & \text{(uniform)} \\ -Vb^2[\frac{1}{2}(\rho/b)^2 - \frac{1}{4}(\rho/b)^4] + \frac{1}{2}\rho^2 & \text{(Poiseuille)}, \end{cases}$$

and
$$\psi^{\infty}_{(c)\,(1)}(\rho) = \tfrac{1}{2}U_{(1)}\rho^2,$$

where I_0, I_1, K_0, and K_1 are the modified Bessel functions of the first and second kind. The above form for $\psi^{(2)}_{(c)\,(i)}(\rho, z)$ is subject to the condition that $V^{(2)}_{(c)\,z(i)}$ and $V^{(2)}_{(c)\,\rho(i)}$ be bounded as $\rho \to 0$ along the rays $z > 1$ and $z < -1$. This condition is difficult to apply. The second integral in (3.2) gives unbounded values for $V^{(2)}_{(c)\,z(i)}$ as $\rho \to 0$ for all z;

elimination of this integral is too restrictive since boundedness is only required for $|z| > 1$.

To circumvent this difficulty, the second integral can be replaced by the Gegenbauer expansion solution of $E^4_{(s)}\psi = 0$, which yields bounded velocities at infinity. Thus

$$\psi^{(2)}_{(c)(i)}(\rho, z) = \psi^{\infty}_{(c)(i)}(\rho) + \int_0^{\infty} \mathrm{d}k\{A_{(i)}(k)\,\rho I_1(k\rho) + B_{(i)}(k)\,\rho^2 I_0(k\rho)\}\cos(kz) + \sum_{n=2}^{\infty} \{E^{(2)}_{n(i)}((\rho^2+z^2)^{(-n+1)/2} + F^{(2)}_{n(i)}((\rho^2+z^2)^{(-n+3)/2}\} C_n^{-\frac{1}{2}}(z/(\rho^2+z^2)^{\frac{1}{2}}) \quad (n \text{ even}). \tag{3.3}$$

The above form constitutes a sufficiently general solution (Leichtberg *et al.* 1976).

The technique used to obtain the constants and the k-functions in (3.1) and (3.3) is outlined as follows. First, the boundary conditions on the tube wall are satisfied exactly, by using the Fourier inverse cosine integral to solve for the unknown coefficients $A(k)$ and $B(k)$ in (3.3). Second, the stream function is rewritten in a compact form in terms of r, θ and the unknown constants $E^{(2)}_{n(i)}$ and $F^{(2)}_{n(i)}$. These two steps are detailed in the Appendix, §A 1, and the stream-function solution which satisfies the wall conditions is given by equation (A 6), and is repeated below:

$$\psi^{(2)}_{(s)(i)}(\theta, r) = \psi^{\infty}_{(s)(i)}(r, \theta) + \sum_{n=2}^{\infty} [E^{(2)}_{n(i)} S^1_n(r, \theta) + F^{(2)}_{n(i)} S^2_n(r, \theta)] \quad (n \text{ even}).$$

A collocation technique is used to satisfy the boundary conditions on the surface of the droplet. The boundary condition $V^{(1)}_{(s)r(i)}(r = 1, \theta) = 0$ ((2.22a), (2.30a)) can be applied directly to (3.1) to eliminate $F^{(1)}_{n(i)}$. Thus the inner solution becomes

$$\psi^{(1)}_{(s)(i)}(r, \theta) = \sum_{n=2}^{\infty} E^{(1)}_{n(i)}(r^n - r^{n+2})\, C_n^{-\frac{1}{2}}(\cos\theta). \tag{3.4}$$

If the other boundary conditions at $r = 1$ ((2.22b, c) and (2.23)) and ((2.30b, c) and (2.26)) are applied to the solutions (A 6) and (3.4), three simultaneous equations in the form of infinite series are obtained. Consider first the clean surface flow or zeroth-order solution. In the collocation technique, the three boundary conditions are satisfied at m discrete points along the surface of the sphere, and the series (A 6) and (3.4) are truncated into a finite form which includes a total of $3m$ terms. A set of $3m$ simultaneous linear algebraic equation is therefore generated and can be solved using any standard matrix reduction technique to obtain the $3m$ unknown constants $E^{(1)}_{n(0)}$, $E^{(2)}_{n(0)}$ and $F^{(2)}_{n(0)}$. The details are given in the Appendix, §A 2.

The first-order solution follows the same procedure of solving unknown coefficients at the zeroth order except that the summations contain p terms, and the Marangoni stress term of (2.27) must be included. $V_{(s)\theta(0)}(\theta)$ up to order $2m$ can be written as

$$V_{(s)\theta(0)}(\theta) = -V\sin\theta\left[1 - \left(\frac{\sin\theta}{b}\right)^2\right] + \sin\theta + \sum_{n=2}^{2m} [E^{(2)}_{n(0)} S^5_n(1, \theta) + F^{(2)}_{n(0)} S^6_n(1, \theta)], \tag{3.5}$$

where the $E^{(2)}_{n(0)}$ and $F^{(2)}_{n(0)}$ have been obtained previously. Using the above expression for $V_{(s)\theta(0)}(\theta)$, the equations that determine the first-order coefficients $E^{(2)}_{n(1)}$, $F^{(2)}_{n(1)}$ and $E^{(1)}_{n(1)}$ can be formulated. These equations are given in the Appendix, §A 3.

An important question arises as to how to choose the location of discrete points on the surface of the droplet to obtain a prescribed accuracy and how to formulate a convergence criterion. Owing to the symmetry in z, collocation points need only be located from $0 \leqslant \theta \leqslant \frac{1}{2}\pi$. Furthermore, since the droplet is moving in a bounded domain, a hydrodynamic influence of the wall on the moving droplet can be significant. This influence is largest at the equator of the droplet and decreases as θ varies from $\frac{1}{2}\pi$ to 0. The points chosen are thus more dense near the equator and less dense near the pole in order to take into account the effect of the wall.

3.2. *Convergence criteria and verification of the method*

As explained in the Introduction, the aim of this study is to compute the hydrodynamic drag on the droplet, and therefore convergence criteria are based on the accurate computation of F'_z. Inserting (A 6) into (2.11*b*) shows that the drag is determined solely by $F^{(2)}_{2(i)}$:

$$F'_{z(i)} = -4\pi a' \mu'^{(2)} U'_0 F^{(2)}_{2(i)}. \tag{3.6}$$

Hydrodynamic drags are usually expressed in terms of drag coefficients λ. Consider first the zeroth order $F^{(2)}_{2(0)}$. For uniform flow, $F^{(2)}_{2(0)}$ is obtained from the solution of (A 9)–(A 11) with $V = 0$. The drag coefficient for uniform flow with no Marangoni stress is denoted by λ_u and is defined as the ratio of F'_z to the force exerted on a droplet moving at U'_0 in an infinite medium. The latter is the Hadamard–Rybczynski value $4\pi' a' \mu'^{(2)} U'_0((1+3\kappa/2)/1+\kappa)$. Thus

$$\lambda_u = F^{(2)}_{2(0)} \frac{1+\kappa}{1+\frac{3}{2}\kappa}. \tag{3.7}$$

For Poiseuille flow, (A 9)–(A 11) indicate that $F^{(2)}_{2(0)}$ is the sum of two contributions, one ($F^{(2)}_{2u(0)}$) derived from the inhomogeneous uniform flow terms (identical to the previous case), and one arising from the inhomogeneous Poiseuille terms. The latter is linear in V, and is denoted by $F^{(2)}_{2v(0)}$ for $V = 1$. The contribution due to the Poiseuille terms gives rise to a drag $-4\pi a' \mu'^{(2)} U'_0 V F^{(2)}_{2v(0)}$. A drag coefficient, λ_v, is defined as this contribution divided by the Hadamard–Rybczynski drag for a sphere moving with velocity V'. Thus

$$\lambda_v = -F^{(2)}_{2v(0)} \frac{1+\kappa}{1+\frac{3}{2}\kappa}, \tag{3.8}$$

where the minus sign is introduced so that λ_v is positive. (The drag due to the Poiseuille flow over a fixed sphere is in the positive z'-direction when V' is larger than zero, and therefore $F^{(2)}_{2v(0)}$ is negative.) The total zeroth-order drag in terms of drag coefficients is

$$F'_{z(0)} = -4\pi a'^{(2)} \left(\frac{1+\frac{3}{2}\kappa}{1+\kappa}\right) [U'_0 \lambda_u - V' \lambda_v]. \tag{3.9}$$

This decomposition reflects the linearity of the zeroth-order problem of Poiseuille flow: the total zeroth-order drag can be thought of as the sum of drags from two flow idealizations, one uniform flow past a fixed sphere with the wall moving at the uniform velocity, and the second Poiseuille flow past a fixed sphere with the wall stationary.

For the first order, it is evident from (2.31) and (A 13)–(A 15) that $F^{(2)}_{2(1)}$ is a sum of three contributions. The first derives from the inhomogeneous $U_{(1)}$ terms in (A 13)

λ	a'/b'	0.1	0.2	0.3	0.4	0.5	0.6	0.7	0.8	0.9
λ_u, λ_v	m	4	4	5	7	7	9	10	11	13
$\lambda_{u(1)}, \lambda_{v(1)}$	p	4	4	5	7	7	9	10	11	13
	m	3	4	5	5	6	6	6	9	10

TABLE 1. The number of collocation points necessary to achieve the accuracy requirement for the gas bubble ($\kappa = 0$)

and is linear in $U_{(1)}$; in fact, for $U_{(1)} = 1$, it is clear that this contribution is identical to $F^{(2)}_{2u(0)}$. The second and third contributions derive from the inhomogeneous Marangoni term in (A 15), and these are linear in ϕ. This inhomogeneous term is itself composed of two sets of terms, one arising from the uniform flow of the zeroth-order state, and one, proportional to V, arising from the Poiseuille flow of the zeroth-order state. Denoting the uniform flow contribution for $\phi = 1$ by $F^{(2)}_{2u(1)}$ and the Poiseuille contribution for $V = 1$ and $\phi = 1$ by $F^{(2)}_{2v(1)}$, drag coefficients may be defined as follows:

$$\lambda_{u(1)} = F^{(2)}_{2u(1)}\left(\frac{1+\kappa}{1+\frac{3}{2}\kappa}\right), \tag{3.10}$$

$$\lambda_{v(1)} = -F^{(2)}_{2v(1)}\left(\frac{1+\kappa}{1+\frac{3}{2}\kappa}\right). \tag{3.11}$$

Thus the complete first-order drag is

$$F'_{z(1)} = -4\pi a' \mu'^{(2)}\left(\frac{1+\frac{3}{2}\kappa}{1+\kappa}\right)\{U'_{(1)}\lambda_u + \phi(U'_0\lambda_{u(1)} - V'\lambda_{v(1)})\} = 0. \tag{3.12}$$

The decomposition of $F'_{z(1)}$ results from the linearity of the first order. The first-order drag can be thought of as the sum of drags from three flow idealizations. The first is the uniform flow (with magnitude $U'_{(1)}$) past a fixed sphere. The second and third are the flows due to the Marangoni surface force term on the left-hand side of (A 15), with $V_{(s)\theta(0)}$ given by the uniform flow contribution in one idealization and by the Poiseuille contribution in the other idealization. One important conclusion from (3.12) concerns the influence of the bulk concentration C'_∞. This parameter only appears in the k non-dimensional group which measures the ratio of adsorption ($\beta' C'_\infty$) to desorption (α'). Note that in the uniformly retarded regime considered, k only appears in the definition of ϕ, as $k/(k+1)$. Since from (3.12) the first-order hydrodynamic drags due to surfactant redistribution are linear in ϕ, the dependence of these drags on the bulk concentration is linear in $k/(k+1)$. Thus when the bulk concentration is equal to zero, no surfactant-related hydrodynamic drags result, and when C'_∞ is large ($k \to \infty$), ϕ is at a maximum, and the largest surfactant influence is obtained.

For the zeroth order, λ_u and λ_v are computed until the difference for successive values of m divided by the previous value is less than 10^{-5}. For $\lambda_{u(1)}$ and $\lambda_{v(1)}$, the same procedure is followed in p with m held fixed, and then m is varied until a precision of 10^{-5} is reached. Table 1 illustrates for $\kappa = 0$ the number of points necessary to achieve this accuracy for λ_u, λ_v, $\lambda_{u(1)}$ and $\lambda_{v(1)}$ as a function of a'/b'. Interestingly, as table 1 indicates, for convergence of the first-order drag coefficients, less collocation points were necessary for the determination of the zeroth-order

			Haberman & Sayre		Wang & Skalak	
a'/b'	λ_u	λ_v	λ_u	λ_v	λ_u	λ_v
0	1.0000	1.0000	1.000	1.000	1.000	1.000
0.1	1.2632	1.2547	1.263	1.255	1.263	1.255
0.2	1.6795	1.6348	1.680	1.635	1.680	1.635
0.3	2.3701	2.2289	2.371	2.231	2.370	2.229
0.4	3.5914	3.2157	3.596	3.218	3.592	3.216
0.5	5.9474	4.9953	5.970	5.004	5.959	4.996
0.6	11.092	8.6130	11.135	8.751	11.10	8.617
0.7	24.676	17.474	24.955	17.671	24.70	17.49
0.8	74.670	47.620	73.555	47.301	74.97	47.81
0.9	469.15	266.37				

TABLE 2. Comparison of converged values of drag coefficients λ_u and λ_v with the results of Haberman & Sayre (1958) and Wang & Skalak (1969) for a solid particle ($\kappa = 10^8$)

				Hyman & Skalak	
a'/b'	κ	λ_u	λ_v	λ_u	λ_v
0.1	0	1.1632	1.1631	1.16	1.16
	1.0	1.2111	1.2063	1.211	1.206
0.2	0	1.3900	1.3895	1.39	1.39
	1.0	1.5209	1.4965	1.520	1.496
0.3	0	1.7251	1.7211	1.725	1.722
	1.0	1.9951	1.9222	1.995	1.922
0.4	0	2.2626	2.2486	2.263	2.241
	1.0	2.7647	2.5820	2.765	2.582
0.5	0	3.2224	3.1295	3.222	3.130
	1.0	4.1197	3.6847	4.123	3.685
0.6	0	5.2043	4.8453	5.205	4.846
	1.0	6.8070	5.7435	6.808	5.744
0.7	0	10.25	8.8356	10.26	8.838
	1.0	13.242	10.321	13.22	10.32
0.8	0	28.615	21.704	28.59	21.72
	1.0	34.450	24.231	34.47	24.26
0.9	0	173.89	109.89		
	1.0	182.98	111.91		

TABLE 3. Comparison of converged values of drag coefficients λ_u and λ_v with the results of Hyman & Skalak's (1970) exact solution for a fluid droplet

surface velocity than were needed for the convergence of the zeroth-order drag coefficients (m for convergence of λ_u and λ_v are larger than m for convergence of $\lambda_{u(1)}$ and $\lambda_{v(1)}$).

This section concludes with a verification of the method. Previous studies by Haberman & Sayre (1958) and Wang & Skalak (1969) have computed λ_u and λ_v for a solid sphere. These values are compared in table 2 with values obtained from this method for $\kappa = 10^8$. The fact that the deviations are all less than 1 % gives confidence in the method. Further verification is obtained by comparing the zeroth-order clean-surface drags for finite values of the droplet viscosity with the results of Hyman & Skalak (1969, 1970). This comparison is detailed in table 3 for $\kappa = 0$ and 1, and a'/b' between 0.1 and 0.8 in increments of 0.1; these are the values of the viscosity ratio and droplet to tube diameter ratio studied by Hyman & Skalak. The agreement is

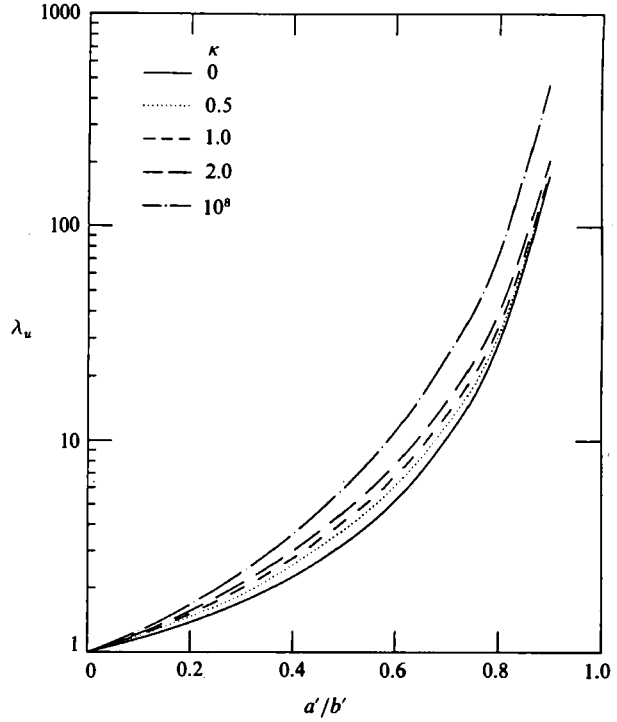

FIGURE 2. Drag coefficient λ_u for uniform flow past a fixed sphere as a function of the ratio of the particle to tube diameters a'/b' for different values of the viscosity ratio κ.

within 0.1 %. Clean-surface drag coefficients as a function of a'/b' for other values of the viscosity ratio ($\kappa = 0.5$ and 2) as well as for $\kappa = 0$, 1.0 and 10^8 are given graphically in figures 2 (for λ_u) and 3 (for λ_v). The hydrodynamic reasons for the trends of these zeroth-order drags are important to the understanding of the first-order surfactant results, and figures 2 and 3 are therefore briefly discussed in the paragraph below.

It is clear from these figures that, for fixed κ, both λ_u and λ_v increase as a'/b' increases. Recall that the drag on the sphere in the flow idealizations that define λ_u and λ_v is equal to a coefficient ξ' ($\xi' = 4\pi a' \mu'^{(2)}(1+\frac{3}{2}\kappa)/(1+\kappa)$) multiplied by $\lambda_u U_0'$ or $\lambda_v V'$. Thus since ξ' is independent of a'/b', the drag (for fixed U_0' or V') increases as a'/b' increases. This is to be expected because, as the gap between the sphere perimeter and the tube wall decreases, the shear rate in the gap in the vicinity of the sphere increases. This results in a higher shear stress being applied to the sphere by the fluid, and the drag consequently increases. A second common characteristic of figures 2 and 3 is the fact that λ_u and λ_v increase with κ at fixed a'/b'. For fixed U_0' or V', the drag also increases because ξ' is a monotonically increasing function of κ varying from 1 to $\frac{3}{2}$. Similar reasoning explains this increase: as the ratio of the droplet to continuous phase viscosity increases, the droplet surface velocity decreases. This reduction in the surface velocity causes the shear rate in the vicinity of the drop to increase, and thus the drag coefficient becomes larger. Finally, the results show that for fixed κ and a'/b', λ_u is always larger than λ_v, and this difference is more pronounced at larger values of a'/b' and κ. From the definitions given in §3.1, it is clear that the drag coefficient for uniform flow is equal (apart from the factor ξ') to the drag for unit velocity at infinity (unit terminal velocity), while the drag

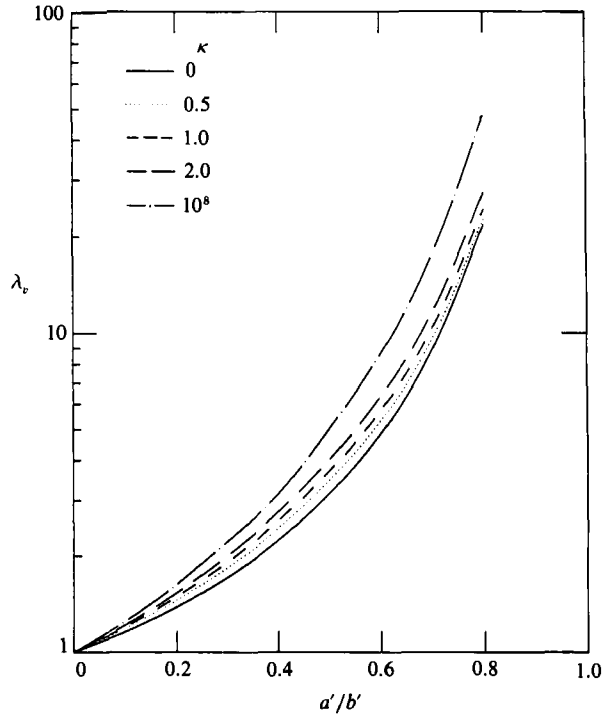

FIGURE 3. Drag coefficient λ_v for Poiseuille flow past a fixed sphere as a function of the ratio of the particle to tube diameters a'/b' for different values of the viscosity ratio κ.

coefficient for Poiseuille flow is directly proportional to the drag for a unit centreline velocity. Thus the flow rate of fluid in the gap between the sphere and tube is, for the case of uniform flow, twice that of Poiseuille flow. This increased flow rate gives rise to a higher shear rate near the sphere, and thus a larger drag. Note that when the gap is very thin (a'/b' large) or the surface velocity is reduced (κ large) this effect is proportionately higher, and it explains the larger differences between λ_u and λ_v as either a'/b' or κ is increased.

4. Surfactant results

4.1. *Hydrodynamic drag*

As explained in §3.2 (cf. (3.12)), the first-order hydrodynamic drag, $F'_{z(1)}$, is composed of three terms. Because of the linearity of the first-order equations, these terms may be interpreted as the drags exerted on the droplet from three separate flow idealizations. The first idealization is the uniform flow, with magnitude $U'_{(1)}$, past a fixed sphere. This drag is dimensionally equal to $-\xi'\lambda_u U'_{(1)}$. The second and third idealizations are the flows caused by the surface force

$$\phi \frac{\partial}{\partial \theta}\left(\frac{1}{\sin\theta}\frac{\partial}{\partial \theta}\sin\theta\, V_{(s)\,\theta(0)}\right),$$

with the wall and the fluid at infinity at rest. The zeroth-order surface velocity $V_{(s)\,\theta(0)}$ appearing in the surface force is the sum of two contributions. The first is the surface velocity that results from uniform flow (with magnitude U'_0) past a fixed sphere. The

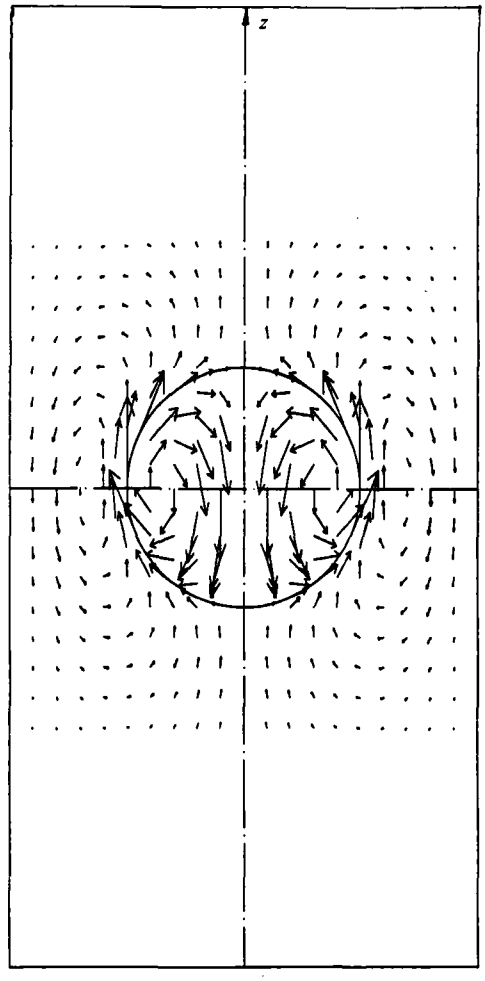

FIGURE 4. First-order non-dimensional velocity distribution due to the Marangoni surface force derived from the zeroth-order uniform flow. The velocity vector is normalized by U_0', and the distribution is for $\kappa = 0.5$, $\phi = 1$ and $a'/b' = 0.5$.

second is the surface velocity that results from Poiseuille flow, with centreline velocity V', past the fixed sphere. The flow idealizations caused by these two contributions to the surface force are discussed below.

For the uniform flow contribution, when $U_0' > 0$, surfactant is convected to the negative z-pole, and therefore a Marangoni stress is directed from the negative z- to the positive z-pole. This traction causes the fluid to move in the positive z-direction, and a balancing hydrodynamic drag in the negative z-direction develops. The dimensional magnitude of this drag is equal to $-\xi'\phi\lambda_{u(1)}U_0'$. The flow idealization caused by the uniform flow contribution to the Marangoni stress is shown in figure 4 for $\phi = 1$, $a'/b' = 0.5$ and $\kappa = 0.5$. This field, and others which follow, is computed in the following manner. A portion of the flow field is divided into a grid. At each of the grid points the velocity is computed from the expression for the stream function ((3.9) and (A 6)). This is undertaken for a particular value of m (or m and p if, as in the case of figure 4, the computation is for a first-order field), and then m and p are increased until a 1% convergence at all of the grid points is achieved. Figure 4

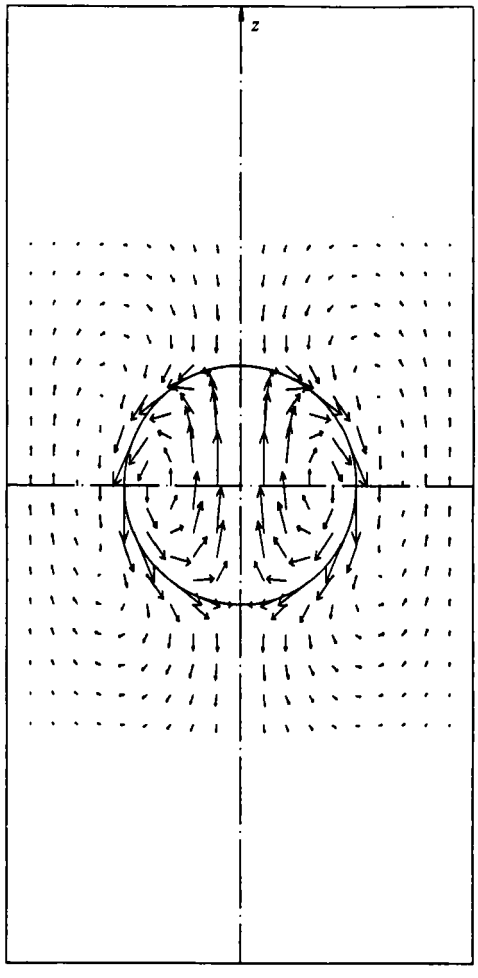

FIGURE 5. First-order non-dimensional velocity distribution due to the Marangoni surface force derived from the zeroth-order Poiseuille flow. The distribution is for $\kappa = 0.5$, $a'/b' = 0.5$, $\phi = 1$ and $V'/U_0' = 1$.

indicates that the magnitude of the fluid velocity is largest at the droplet surface. This high surface velocity is because the driving force is being exerted on the surface. Also note from the figure that a recirculation develops in the gap between the sphere and the tube wall since the flow at infinity is equal to zero.

The second contribution to the zeroth-order surface velocity in the Marangoni stress term is that due to the Poiseuille flow. When $V' > 0$, the Poiseuille flow convects surfactant to the positive z-pole and therefore a Marangoni stress is created which is directed from the positive to the negative pole. This causes fluid to move in the minus z-direction, and an equalizing hydrodynamic drag develops in the positive z-direction. The magnitude of this drag is equal to $\xi'\phi\lambda_{v(1)}V'$. The flow idealization for the Poiseuille-induced surface force is given in figure 5, again for $\phi = 1$, $\kappa = 0.5$ and $a'/b' = 0.5$ (also $V'/U_0' = 1$). The structure is similar to the field induced by the uniform flow, but the magnitude of the velocities is uniformly smaller. This can be explained as follows. For $V'/U_0' = 1$, the flow rate in the gap between the sphere and the tube wall for uniform flow is twice as large as that for Poiseuille flow. Since the flow rate is larger the change in the average velocity between the entrance and exit

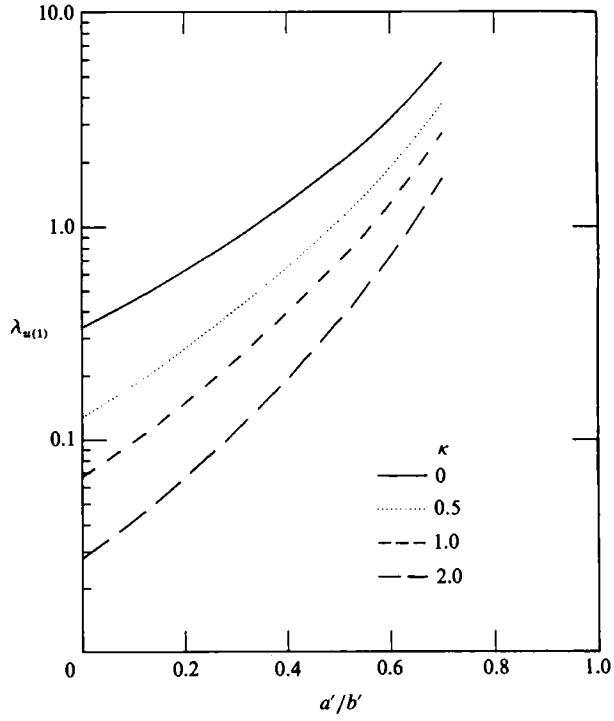

FIGURE 6. First-order drag coefficient correction $\lambda_{u(1)}$ for the surface Marangoni force corresponding to the uniform zeroth-order flow as a function of a'/b' for different values of κ.

to the gap, and the gap centre, is much larger for uniform flow than for Poiseuille flow. Therefore the surface gradient of velocity and thus the dilatation is larger. Since the dilatation is proportional to the surface force it too is larger for the uniform flow and thus the velocities arising from the surface force for this case are larger.

The converged results for $\lambda_{u(1)}$ and $\lambda_{v(1)}$ are given, respectively, in figures 6 and 7 for $\kappa = 0$, 0.5, 1 and 2 and the gap ratio a'/b' in the range 0.1 to 0.7. From these figures it is clear that $\lambda_{u(1)}$ and $\lambda_{v(1)}$ are increasing functions of a'/b' and decreasing functions of κ. (Parenthetically note also that when $\lambda_{u(1)}$ and $\lambda_{v(1)}$ are multiplied by ξ' (which itself increases monotonically with κ), the result is $\xi'\lambda_{u(1)}\phi U_0'$, $\xi'\lambda_{v(1)}\phi V'$ and thus the actual first-order drag due to the surface forces still decreases with κ with $U_0'\phi$ and $V'\phi$ held constant.) The fact that the Marangoni drag caused by the surface forces increases with a'/b' and decreases with κ can be explained as follows. As the ratio of the droplet to the continuous phase viscosity increases or the sphere to tube diameter decreases, the circulation within the droplet is diminished and the surface dilatation $((1/\sin\theta)(\partial/\partial\theta)\sin\theta V_{(s)\theta(0)})$ is reduced. The reduction in the dilatation causes a decrease in the surface force which drives the flows in the two idealizations with respect to which $\lambda_{u(1)}$ and $\lambda_{v(1)}$ are defined, and this results in a decrease in the drag. Finally note from figures 6 and 7 that as a'/b' tends to zero, $\lambda_{u(1)}$ approaches $\lambda_{v(1)}$. This is to be expected since as $a'/b' \to 0$, the zeroth-order surface velocities for uniform and Poiseuille flow become equal. (Recall that in this limit, λ_u approaches λ_v.)

As remarked in the Introduction, there have been no attempts in the literature to examine the hydrodynamic drag exerted on fluid particles in tubes for the case in which surfactants are adsorbed onto the fluid particle surfaces. However, the

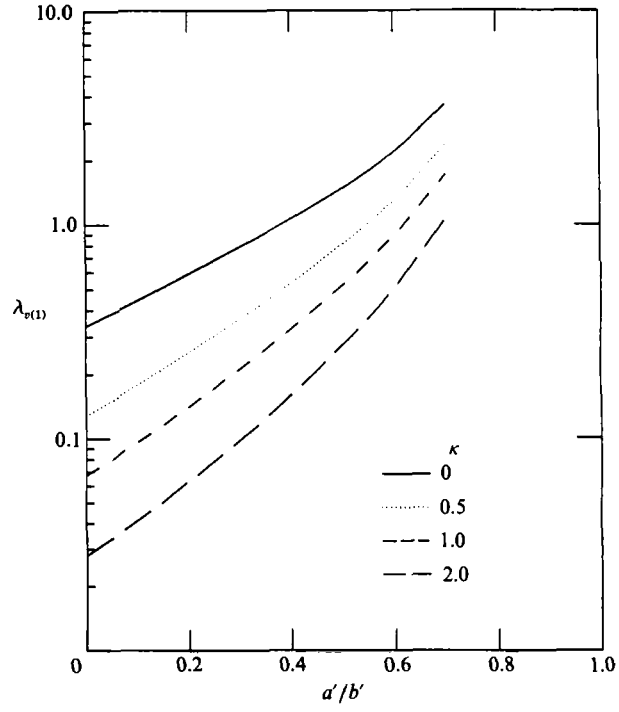

FIGURE 7. First-order drag coefficient correction $\lambda_{v(1)}$ for the surface Marangoni force corresponding to the zeroth-order Poiseuille flow as a function of a'/b' for different values of κ.

influence of surfactants on the drag exerted on particles in an infinite medium has been studied extensively and these studies may be used to verify the present results. In particular, for the case described in §2.2 in which sublayer–surface kinetic exchange is fast, but rate limiting, Levich (1962) derived the following expression for $\lambda_{u(1)}$:

$$\lambda_{u(1)} = \frac{\left(2 - \dfrac{1+2\kappa}{1+\kappa}\right)}{3(1+\frac{3}{2}\kappa)}. \tag{4.1}$$

Values from Levich's expression should agree with the converged values of $\lambda_{u(1)}$ as given in figure 6 as a'/b' tends to zero since in this limit the hydrodynamic effect of the wall on the drag becomes negligible. The values from Levich's expression for $\kappa = 0$, 0.5, 1 and 2 are, respectively, 0.333, 0.127, 0.0667, and 0.0278. These values agree with the asymptotes in the figure, and this agreement provides a check of the first-order results.

4.2. *First-order terminal velocities*

With the hydrodynamic drag determined, terminal velocities for different circumstances can be computed. Three cases are considered here: (i) the motion of a drop in a vertical tube due only to gravity, (ii) the motion of a neutrally buoyant drop suspended in Poiseuille flow and (iii) the motion of a drop in a vertical tube due to gravity and Poiseuille flow. These are considered separately in the following.

The first case is that of the motion due to gravity of a droplet in a vertical tube with the fluid at rest far away from the drop. Consider first the zeroth order. The (zeroth-order) force exerted on the drop is equal to $\frac{4}{3}\pi a'^3(\rho'^{(1)} - \rho'^{(2)})g'$. Summing this

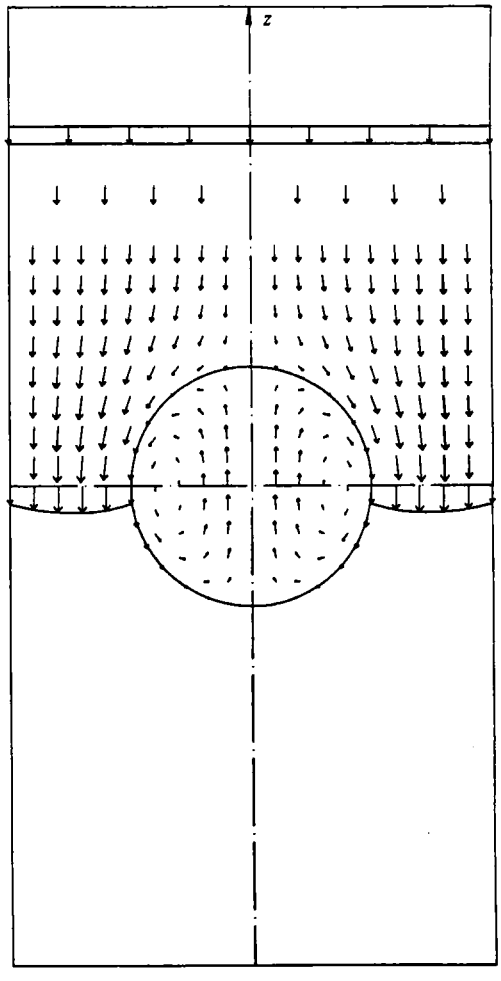

FIGURE 8. Presentation of the clean-surface non-dimensional velocity field for uniform flow past a fixed sphere. This field is for $\kappa = 0.5$ and $a'/b' = 0.5$.

force with the hydrodynamic drag as given in (3.9) with $V' = 0$ yields $-U'_0 \lambda_u \xi' - \frac{4}{3}\pi a'^3(\rho'^{(1)} - \rho'^{(2)})\, g = 0$, and therefore the following equation for U'_0 is obtained:

$$\frac{U'_0}{U'_{\text{H-R}}} = \frac{1}{\lambda_u}, \tag{4.2}$$

where $U'_{\text{H-R}}$ denotes the Hadamard–Rybczynski gravitational terminal velocity in an infinite medium and is

$$U'_{\text{H-R}} = -\frac{a'^2(\rho'^{(1)} - \rho'^{(2)})\, g'}{3\mu'^{(2)}}\left(\frac{1+\kappa}{1+\frac{3}{2}\kappa}\right). \tag{4.3}$$

An illustration of the velocity field for this case for $a'/b' = 0.5$ and $\kappa = 0.5$ is given in figure 8 in the reference frame in which the sphere is stationary.

For the first order, the drag is zero and thus, from (3.12)

$$-U'_{(1)} \lambda_u - \phi U'_0 \lambda_{u(1)} = 0 \tag{4.4}$$

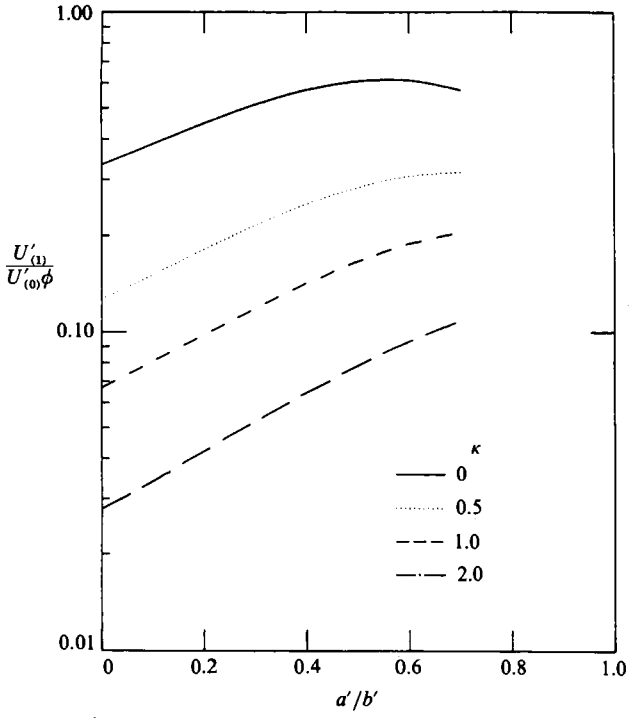

FIGURE 9. The first-order velocity correction for a surfactant-laden droplet moving under buoyancy in a tube filled with a still fluid as a function of a'/b' for different values of κ.

or
$$\frac{U'_{(1)}}{U'_0} = -\phi\left(\frac{\lambda_{u(1)}}{\lambda_u}\right). \tag{4.5}$$

Note that since $U'_{(1)}$ is of opposite sign to U'_0, the presence of a surfactant reduces the droplet speed. A graphical representation of the dependence of $-U'_{(1)}/(\phi U'_0)$ on a'/b' for $\kappa = 0$, 0.5, 2 and 2 is given in figure 9. (Note that $\phi U'_0$ is not a function of a'/b' or κ). The figure indicates that the relative correction is a decreasing function of κ. This is to be expected since λ_u increases with κ, and $\lambda_{u(1)}$ decreases with κ. Thus $\lambda_{u(1)}/\lambda_u$ must decrease with κ. The figure also shows that $-U'_{(1)}/(\phi U'_0)$ is an increasing function of a'/b' for $a'/b' < 0.5$. After this point, as a'/b' increases the curves level off, and for $\kappa = 0$, begin to decrease. These results reflect the fact that for $a'/b' < 0.5$, $\lambda_{u(1)}$ increases faster with a'/b' than does λ_u, but after 0.5 the reverse begins to be true. Apparently, as the ratio of sphere to tube diameter increases, at first the increase in the Marangoni drag $\lambda_{u(1)}$ due to increasing a'/b' overcompensates for the increase in the drag λ_u which resists the Marangoni-induced motion, but eventually the increasing effect of a'/b' on λ_u becomes controlling.

For the gravity-driven flow, the first-order surfactant distribution ($\Gamma_{(1)}$) may be obtained from (2.25). A graph of $\Gamma_{(1)}\nu^*(1+k)$ for $\kappa = 0.5$ and $a'/b' = 0.5$ is presented in figure 10 (dashed line). The graph exhibits the accumulation of surfactant at the downstream pole ($\theta = \pi$) due to the zeroth-order flow and is antisymmetric with respect to $\theta = \frac{1}{2}\pi$ because of the symmetry in the velocity field (cf. the discussion at the beginning of §3).

The second case is the motion of a neutrally buoyant sphere in Poiseuille flow. In this case no force is exerted on the drop, and the hydrodynamic drag is equal to zero.

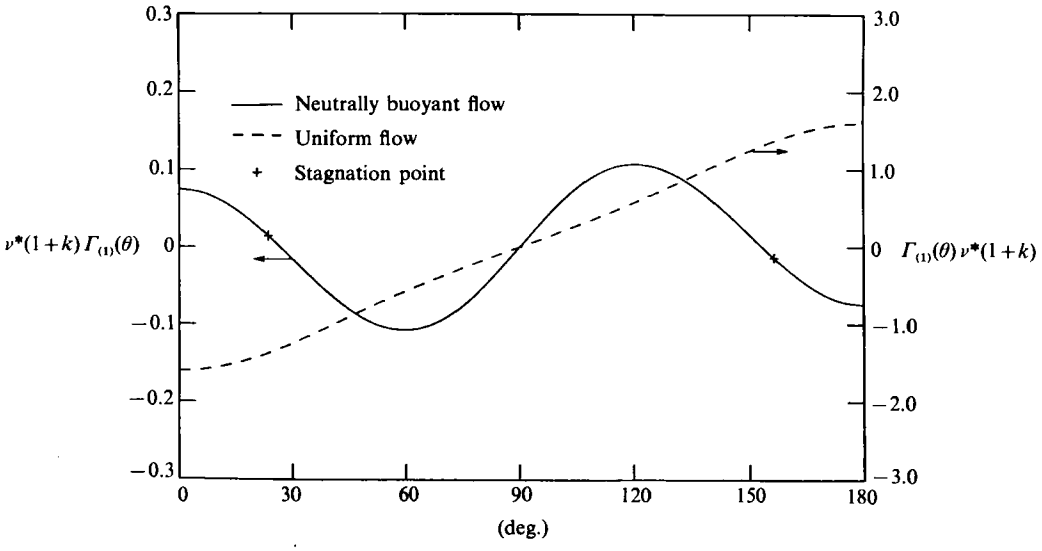

FIGURE 10. The first-order correction for the surfactant distribution for buoyancy-driven motion in a still liquid and for a neutrally buoyant particle suspended in Poiseuille flow ($\kappa = 0.5$, $a'/b' = 0.5$).

Setting $F'_{z(1)} = 0$ in (3.9) yields the relationship between U'_0, the steady droplet velocity, and V', the centreline velocity of the Poiseuille flow:

$$\frac{U'_0}{V'} = \frac{\lambda_v}{\lambda_u}. \tag{4.6}$$

Since $\lambda_v < \lambda_u$, the terminal velocity U'_0 is always less than the centreline velocity V'. Note also that λ_v/λ_u is a decreasing function of κ and a'/b' since, as discussed above, the disparity between λ_v and λ_u increases as either a'/b' or κ is increased. Thus the terminal velocity of a fluid droplet suspended in a Poiseuille flow will decrease relative to the Poiseuille centreline velocity V' as either κ or a'/b' is increased. Illustrations of the flow field for this case (non-dimensionalized by U'_0) are given in figures 11 (*a*) and 11 (*b*) for $\kappa = 0.5$ and $a'/b' = 0.5$ in the frame in which the drop is stationary and the wall is moving at unit velocity.

The flow fields of figures 11 (*a*) and 11 (*b*) show the recirculation of the continuous phase at the front and back of the drop due to the fact that the terminal velocity is less than the centreline velocity. The stagnation rings on the surface of the sphere, which are caused by the recirculation are shown clearly in the enlargement (figure 11 *b*). For decreasing values of U'_0/V' (for example due to increasing κ), the rings move towards the equator ($\theta = \frac{1}{2}\pi$) as the recirculation becomes more pronounced. This trend is shown in table 4 where the location of the upstream stagnation ring is detailed as a function of κ for $a'/b' = 0.5$.

Since the force on the drop is zero for this case, $F'_{z(1)} = 0$, and (3.12) may be used to solve for $U'_{(1)}$. The result is

$$\frac{U'_{(1)}}{U'_0} = -\phi\left(\frac{\lambda_{u(1)}}{\lambda_u} - \frac{\lambda_{v(1)}}{\lambda_v}\right), \tag{4.7}$$

where use has been made of the zeroth-order result $U'_0 = (\lambda_v/\lambda_u)\,V'$ to eliminate V'. Graphs of $-U'_{(1)}/(\phi U'_{(0)})$ as a function of a'/b' for $\kappa = 0$, 0.5, 1 and 2 are given in

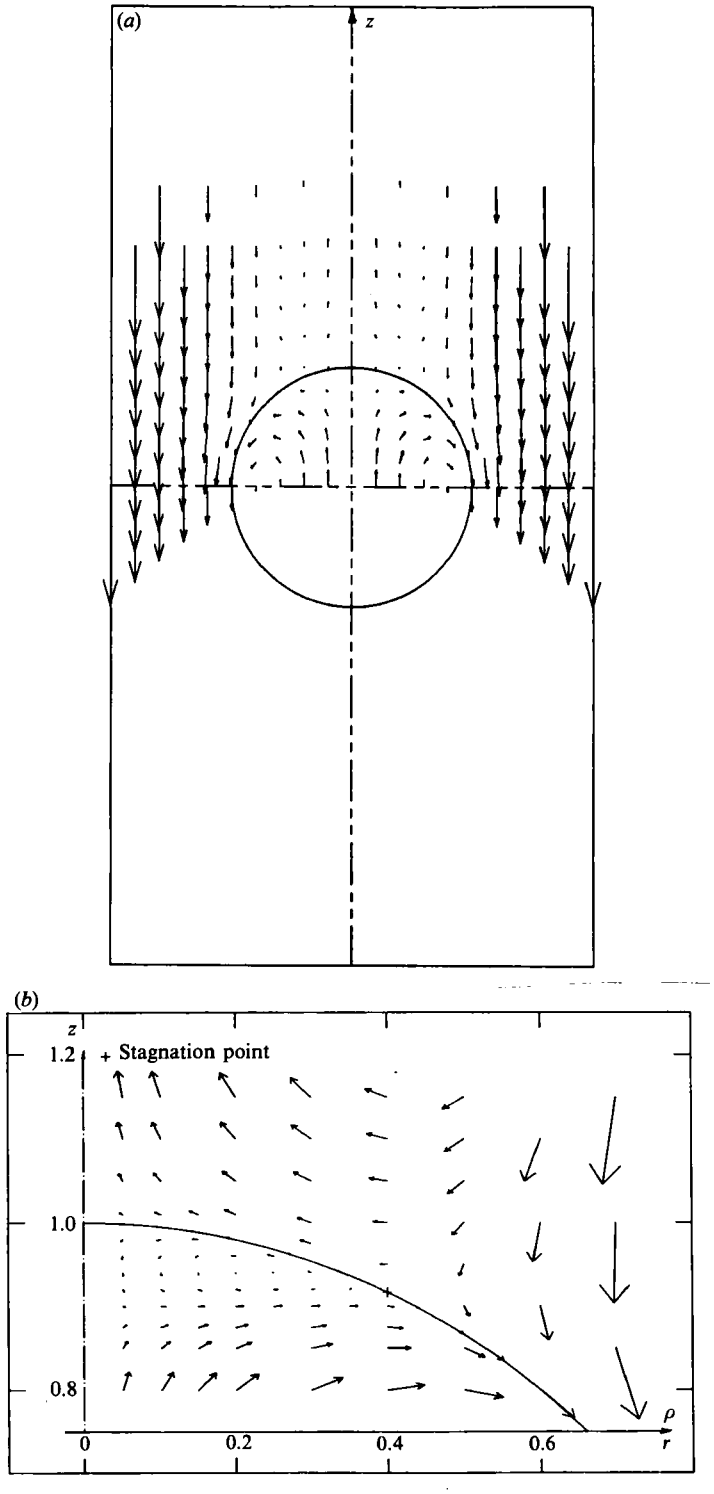

FIGURE 11. (*a*) Clean-surface non-dimensional velocity field for a neutrally buoyant fluid particle in a frame for which the particle is stationary. This field is for $\kappa = 0.5$, $a'/b' = 0.5$, and $\bar{V}'/U_0' = \lambda_u/\lambda_v$. (*b*) Enlargement of the upstream pole of the field detailed in (*a*) showing the recirculation in the continuous phase and the location of the stagnation ring on the surface.

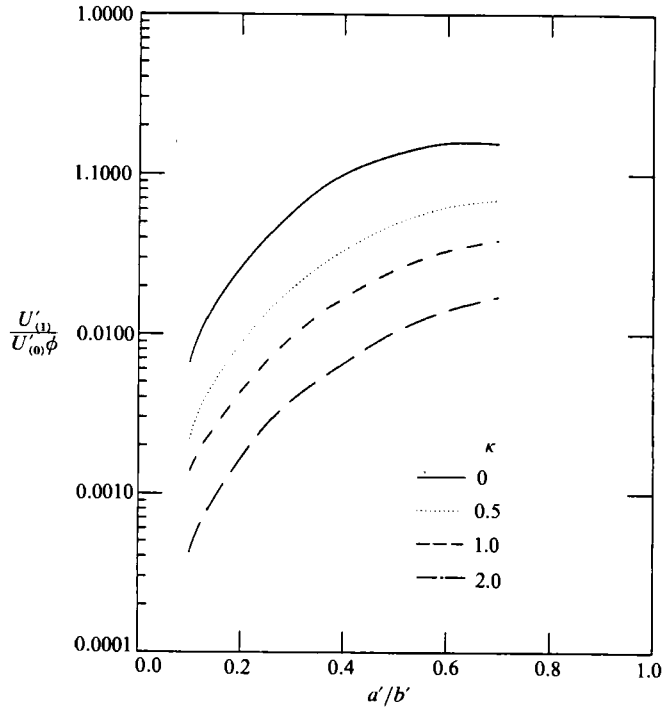

FIGURE 12. The first-order velocity for a neutrally buoyant surfactant-laden droplet moving in a tube as a function of a'/b' and κ.

κ	$\frac{u'_0}{V'}$	θ (deg.)	$\frac{-U'_{(1)}}{U'_0\phi}$
	(*a*) Neutrally buoyant		
0	0.9712	14.84	0.1335
0.5	0.9169	23.58	0.0491
1.0	0.8944	26.59	0.0254
2.0	0.8743	29.10	0.0104
(*b*) Suspended droplet acted upon by Buoyancy ($\kappa = 0.5$)			
0.5	0.85	41.10	0.0076
	0.80	54.16	−0.0096
	0.75	72.50	−0.1077

TABLE 4. Angular location of the upstream stagnation ring ($a'/b' = 0.5$)

figure 12. The graphs indicate that $-U'_{(1)}/(\phi U'_{(0)}) > 0$ for the values of a'/b' and κ used, and therefore the droplet speed is once again retarded because of the surfactant adsorption. The dependencies of the correction on a'/b' and κ are similar to that for the gravity-driven motion (figure 9).

The first-order surfactant distribution for the motion of a neutrally buoyant sphere in Poiseuille flow is given in figure 10 (solid line) for κ and a'/b' equal to 0.5. This figure should be compared with the zeroth-order velocity field as given in figures 11 (*a*) and 11 (*b*). Because of the zeroth-order flow, surfactant is swept away from the

stagnation ring at 23.58° and the downstream pole, and towards the upstream pole and the stagnation ring at 156.42°. This causes the accumulation of surfactant at the upstream pole and the 156.42° ring and a depletion in the other two stagnation areas. Note importantly that even in this first-order theory, the minima and maxima do not occur precisely at the stagnation zones but are offset from these. This is because (from (2.25)) extreme behaviour in $\Gamma_{(1)}$ occurs when the dilatation is at a minimum or maximum, not when the surface velocity is zero.

The last case is a droplet moving due to gravity in a vertical tube with Poiseuille flow at infinity. The zeroth-order force balance is

$$(V'\lambda_v - U_0'\lambda_u)\xi' - \tfrac{4}{3}\pi a'^3(\rho'^{(1)} - \rho'^{(2)})g' = 0, \tag{4.8}$$

from which the terminal velocity U_0' may be computed in terms of the centreline Poiseuille velocity and the gravitational force. Thus

$$\frac{U_0'}{V'} = \frac{1}{\lambda_u}\frac{U'_{\text{H-R}}}{V'} + \frac{\lambda_v}{\lambda_u}. \tag{4.9}$$

It is clear from (4.9) that U_0'/V' may take on any value depending on the ratio $U'_{\text{H-R}}/V'$. As $U'_{\text{H-R}}/V'$ decreases from zero and tends to $-\lambda_v$ (the value that arrests the sphere), U_0'/V' decreases from the neutrally buoyant value (λ_v/λ_u) towards zero. The stagnation ring moves from the neutrally buoyant location towards the equator ($\theta = \frac{1}{2}\pi$). This behaviour is detailed in table 4(*a*) for $\kappa = 0.5$ and $a'/b' = 0.5$.

Again from (3.12) with $F'_{z(1)} = 0$, the first-order velocity may be obtained. The result is

$$\frac{U'_{(1)}}{U_0'} = -\phi\left\{\frac{\lambda_{u(1)}}{\lambda_u} - \frac{\lambda_{v(1)}}{\lambda_u}\frac{V'}{U_0'}\right\} \tag{4.10}$$

for a given value of V'/U_0'. This latter ratio, obtained from (4.9) is a function of $U'_{\text{H-R}}$ and may take on any value depending on $U'_{\text{H-R}}/V'$. Several cases are possible, and these are discussed in the following paragraphs.

If the buoyancy force and the centreline velocity are in the same direction, then $U'_{\text{H-R}}/V' > 0$. From (4.9) it is clear that for this case $U_0'/V' > 0$ and is larger than the neutrally buoyant value. From (4.10), $U'_{(1)}/U_0' < 0$ and, in fact, is larger (in absolute value) than the neutrally buoyant value. Thus for this case the drop is retarded even more than for the case of the neutrally buoyant sphere. The reason is clear. As $U'_{\text{H-R}}/V'$ increases from zero, U_0'/V increases from the neutrally buoyant value and the stagnation rings approach the poles. The regions on the surface of Marangoni stress that cause acceleration of the drop disappear, and thus retardation is increased.

Consider next the case in which the buoyancy force is in the opposite direction to that of the Poiseuille centreline velocity ($U'_{\text{H-R}}/V' < 0$) but larger than $-\lambda_v$ (the value that arrests the clean sphere translation). Then U_0'/V' is still larger than zero (see (4.9)), but smaller than the neutrally buoyant value of λ_v/λ_u. As $U'_{\text{H-R}}/V'$ tends to $-\lambda_v$, U_0'/V' tends to zero (see (4.9)) and (4.7) indicates that $U'_{(1)}/U_0'$ will become larger than zero. Thus droplet acceleration can be realized in the limit in which $U'_{\text{H-R}}/V'$ tends to $-\lambda_v$ and U_0'/V consequently becomes vanishingly small. The reason is that as $U'_{\text{H-R}}/V'$ approaches $-\lambda_v$, the stagnation rings approach $\frac{1}{2}\pi$ and the Marangoni stresses that accelerate the drop increase at the expense of those that retard the translation. Hence the eventual increase in speed with surfactant adsorption. This behaviour is illustrated in table 4(*b*) for $\kappa = 0.5$ and $a'/b' = 0.5$.

Finally, for the case in which the buoyancy and the centreline velocity are in opposite directions ($U'_{\text{H-R}}/V' < 0$) and $U'_{\text{H-R}}/V' < -\lambda_v$, U'_0/V' becomes less than zero (see (4.9)) and the sphere moves opposite to the Poiseuille flow. The surfactant distribution increases monotonically towards the downstream pole (now at $\theta = 0$) and Marangoni stresses simply retard the speed ($U'_{(1)}/U'_0 < 0$, equation (4.10)).

5. Conclusions

This study has focused on the determination of the hydrodynamic drag exerted on a spherical fluid particle in a tube for the case in which the particle interface is covered by surfactant adsorbed from the continuous liquid phase filling the tube. To compute the influence of the adsorbed monolayer on the hydrodynamic drag, the surface surfactant distribution must be determined so as to calculate the interfacial tension gradient or Marangoni force. In this study a perturbative approach was adopted which simplifies the determination of the surfactant surface concentration by isolating in a simplified way one non-convective transport mechanism, kinetic exchange. In this approach, the kinetic exchange of surfactant at the interface by desorption is assumed to be much faster than the rate of convection of surfactant from one pole of the drop to the other ($\nu = O(1/\epsilon)$). Diffusion of surfactant in the bulk is relegated to higher-order effects by the assumption that the adsorption depth is sufficiently small. Within this perturbation scheme, to order zero in ϵ, the surface surfactant concentration was shown to be uniform, and the drag was therefore described by the clean-surface drag coefficients λ_u and λ_w.

The first-order surfactant distribution is determined solely by the zeroth-order surface dilatation. The first-order drag coefficients were computed from the Marangoni surface force corresponding to the first-order surfactant distribution. The solutions obtained for the flow due to the Marangoni surface force may be viewed in a general way since the flow due to any arbitrary surface force may be obtained from the framework by replacing the ϕ-term on the left-hand side of (A 15) with the arbitrary surface force exerted as a function of θ.

The results for uniform flow resembled those for uniform flow past a spherical droplet in an infinite medium: the only stagnation regions along the clean surface are at the poles (figure 8); surfactant molecules collect at the downstream stagnation pole (figure 10), and the resulting Marangoni stress retards the terminal velocity ($U'_{(1)}/U'_0 < 0$, figure 9). The interesting point with regard to the uniform results is that the retardation at first increases with a'/b', and then becomes modulated and may even decrease (for small κ) for larger a'/b' (cf. figure 9).

The most interesting surfactant results were obtained for particles placed in Poiseuille flow. For neutrally buoyant particles the zeroth-order flow exhibited two stagnation points at the poles and two stagnation rings (figures 11*a* and 11*b*). The surface flow for this case is such that fluid moves away from the upstream stagnation ring and downstream pole and towards the upstream pole and downstream stagnation ring. It is important to note that the backflow towards the upstream stagnation point and away from the downstream pole is due to the Poiseuille component of the flow at infinity. As the centreline velocity V' increases relative to U'_0, the stagnation rings move towards $\theta = \frac{1}{2}\pi$ (table 4). As a result of the zeroth-order surface velocity distribution, surfactant accumulates in the first-order state at the upstream pole and downstream stagnation ring and is depleted at the other stagnation zones (figure 10). Between the upstream stagnation ring and upstream pole a Marangoni tension in the minus z-direction is created. The same is true

between the downstream pole and downstream stagnation ring. These Marangoni tractions are balanced by stresses exerted in the positive z-direction by the liquid surrounding the fluid particle. Such stresses accelerate the particle, and therefore tend to make $U'_{(1)}/U'_0 > 0$. Between the downstream and upstream rings a Marangoni tension in the positive z-direction arises, and a balancing continuous fluid drag decelerates the particle as it acts in the minus z-direction. These effects are reflected in (4.10) where the first term on the right-hand side accounts for the retarding stress of the region between the rings and the second term represents the accelerating stresses of the ring to pole regions. For the case of the neutrally buoyant particle, the relationship beween V' and U'_0 is such that the decelerating effects predominate and the velocity is retarded (figure 12), but as U'_0/V' tends to zero (as a result of gravity acting in a direction opposite to the drag of the Poiseuille flow), first-order acceleration is possible as the stagnation rings move further towards the equator (table 4).

This research has been supported in part by a Department of Energy Grant for Basic Sciences (DE-FG02-88ER13820) and a National Science Foundation Grant (CPE-8404261).

Appendix. Some details of the solution construction and boundary conditions

A.1. *Construction of solutions satisfying the wall conditions*

Using (3.3), the boundary condition ((2.22a) or (2.29a)) becomes

$$\int_0^\infty \mathrm{d}k\{A_{(i)}(k)\, kI_0(bk) + B_{(i)}(k)\{bkI_1(bk) + 2I_0(bk)]\}\cos(kz) = -\sum_{n=2}^{\infty} [E^{(2)}_{n(i)}\, G^1_n(z) + F^{(2)}_{n(i)}\, G^2_n(z)]. \quad \text{(A 1)}$$

Instead of using $V^{(2)}_{(c)\rho(i)}(\rho = b) = 0$ ((2.21b), (2.29b)), the equivalent condition $\psi^{(2)}_{(c)(i)}(\rho = b) = \psi^{\infty}_{(c)(i)}(b)$ is applied for convenience. That is

$$\int_0^\infty \mathrm{d}k\{A_{(i)}(k)\, bI_1(bk) + B_{(i)}(k)\, b^2 I_0(bk)\}\cos(kz) = -\sum_{n=2}^{\infty} [E^{(2)}_{n(i)}\, G^3_n(z) + F^{(2)}_{n(i)}\, G^4_n(z)], \quad \text{(A 2)}$$

where, for $j = 1, 2, 3, 4$, $G^j_n(z)$ are of the form

$$\left.\begin{aligned} G^1_n(z) &= (b^2+z^2)^{-(n+1)/2} P_n\left[\frac{z}{(b^2+z^2)^{\frac{1}{2}}}\right], \\ G^2_n(z) &= (b^2+z^2)^{-(n-1)/2}\left\{P_n\left[\frac{z}{(b^2+z^2)^{\frac{1}{2}}}\right] + 2C_n^{-\frac{1}{2}}\left[\frac{z}{(b^2+z^2)^{\frac{1}{2}}}\right]\right\} \\ G^3_n(z) &= (b^2+z^2)^{-(n-1)/2} C_n^{-\frac{1}{2}}\left[\frac{z}{(b^2+z^2)^{\frac{1}{2}}}\right], \\ G^4_n(z) &= (b^2+z^2)^{-(n-3)/2} C_n^{-\frac{1}{2}}\left[\frac{z}{(b^2+z^2)^{\frac{1}{2}}}\right]. \end{aligned}\right\} \quad \text{(A 3)}$$

In the above, spherical coordinates (r, θ) have been transformed into cylindrical

coordinates (ρ, z). The boundary conditions (A 1) and (A 2) can be inverted by the inverse Fourier cosine transform to solve for $A(k)$ and $B(k)$. Integrating the inverse integrals yields

$$\left.\begin{aligned} A_{(i)}(k)\,kI_0(bk)+B_{(i)}(k)[bkI_1(bk)+2I_0(bk)] &= -\sum_{n-2}^{\infty}[E^{(2)}_{n(i)}H^1_n(k)+F^{(2)}_{n(i)}H^2_n(k)],\\ A_{(i)}(k)\,bI_1(bk)+B_{(i)}(k)\,b^2I_0(bk) &= -\sum_{n-2}^{\infty}[E^{(2)}_{n(i)}H^3_n(k)+F^{(2)}_{n(i)}H^4_n(k)], \end{aligned}\right\} \tag{A 4}$$

where $H^j_n(k), j = 1,2,3,4$, are given as (Leichtberg *et al.* 1976)

$$\left.\begin{aligned} H^1_n(k) &= (-1)^{n/2}\frac{2}{\pi n!}k^nK_0(bk),\\ H^2_n(k) &= -(-1)^{n/2}\frac{2}{\pi n!}k^{n-2}[n(n-1)K_0(bk)-(2n-3)\,bkK_1(bk)],\\ H^3_n(k) &= -(-1)^{n/2}\frac{2}{\pi n!}bk^{n-1}K_1(bk),\\ H^4_n(k) &= -(-1)^{n/2}\frac{2}{\pi n!}bk^{n-3}[(2n-3)\,bkK_0(bk)-(n-2)(n-3)K_1(bk)]. \end{aligned}\right\} \tag{A 5}$$

$A(k)$ and $B(k)$ can be solved in terms of the unknown constants $E^{(2)}_{n(i)}$ and $F^{(2)}_{n(i)}$. With $A_{(i)}(k)$ and $B_{(i)}(k)$ determined, the stream function can be written in a new compact form in spherical coordinates as follows:

$$\psi^{(2)}_{(s)(i)}(\theta, r) = \psi^{\infty}_{(s)(i)}(r,\theta)+\sum_{n-2}^{\infty}[E^{(2)}_{n(i)}S^1_n(r,\theta)+F^{(2)}_{n(i)}S^2_n(r,\theta)]. \tag{A 6}$$

In the above

$$\left.\begin{aligned} S^1_n(r,\theta) &= r^{-n+1}C^{-\frac{1}{2}}_n(\cos\theta)+\int_0^{\infty}\mathrm{d}k\cos(kr\cos\theta)\{T^1_n(k)\,r\sin\theta I_1(kr\sin\theta)\\ &\quad + T^3_n(k)(r\sin\theta)^2I_0(kr\sin\theta)\},\\ S^2_n(r,\theta) &= r^{-n+3}C^{-\frac{1}{2}}_n(\cos\theta)+\int_0^{\infty}\mathrm{d}k\cos(kr\cos\theta)\{T^2_n(k)\,r\sin\theta I_1(kr\sin\theta)\\ &\quad + T^4_n(k)(r\sin\theta)^2I_0(kr\sin\theta)\}. \end{aligned}\right\} \tag{A 7}$$

The $T^i_n(k)$ functions $(i = 1,2,3,4)$ appearing in (A 7) are defined as

$$\left.\begin{aligned} T^1_n(k) &= \frac{(2+bk\Omega)H^3_n(k)-b^2H^1_n(k)}{\Delta}, \quad T^2_n(\kappa) = \frac{(2+\beta\kappa\Omega)H^4_n(k)-b^2H^2_n(k)}{\Delta},\\ T^3_n(k) &= \frac{b\Omega H^1_n(k)-kH^3_n(k)}{\Delta}, \quad T^4_n(k) = \frac{b\Omega H^2_n(k)-kH^4_n(k)}{\Delta}, \end{aligned}\right\} \tag{A 8}$$

where Ω and Δ are defined

$$\Omega = \frac{I_1(kb)}{I_0(kb)}, \quad \Delta = b^2kI_0(bk)-2bI_1(bk)-b^2kI_1(bk)\,\Omega.$$

The integrals in (A 7) must be evaluated numerically once r and θ are specified.

A.2. *Collocation conditions on the sphere surface (zeroth order)*

When the zeroth-order (tangentially free) boundary conditions on the surface of the sphere are satisfied at m points on the first quadrant of the sphere surface, the $3m$ truncated equations from boundary conditions (2.22b, c) and (2.23) are given as

$$V\cos\theta_i\left[1-\left(\frac{\sin\theta_i}{b}\right)^2\right]-\cos\theta_i=\sum_{n=2}^{2m}[E^{(2)}_{n(0)}S^3_n(1,\theta_i)+F^{(2)}_{n(0)}S^4_n(1,\theta_i)], \tag{A 9}$$

$$V\sin\theta_i\left[1-\left(\frac{\sin\theta_i}{b}\right)^2\right]-\sin\theta_i=\sum_{n=2}^{2m}[E^{(2)}_{n(0)}S^5_n(1,\theta_i)+F^{(2)}_{n(0)}S^6_n(1,\theta_i)+\frac{2}{\sin\theta_i}E^{(1)}_{n(0)}C_n^{-\frac{1}{2}}(\cos\theta_i)], \tag{A 10}$$

$$V\sin\theta_i\left[1+\left(\frac{\sin\theta_i}{b}\right)^2\right]-\sin\theta_i=\sum_{n=2}^{2m}[E^{(2)}_{n(0)}S^7_n(1,\theta_i)+F^{(2)}_{n(0)}S^8_n(1,\theta_i)-\frac{2(2n-1)\kappa}{\sin\theta_i}E^{(1)}_{n(0)}C_n^{-\frac{1}{2}}(\cos\theta_i)], \tag{A 11}$$

where i denotes the collocation point ($i=1,2,\ldots,m$) and the $S^q_n(1,\theta_i)$ are given below. The above equations are valid for Poiseuille flow at infinity. The equations valid for uniform flow may be obtained from these by letting $V=0$:

$$\begin{aligned}
\begin{bmatrix}S^3_n\\S^4_n\end{bmatrix}&=P_{n-1}(\cos\theta)+\int_0^\infty dk\Big\{k\sin(k\cos\theta)\Big[\begin{bmatrix}T^1_n\\T^2_n\end{bmatrix}\sin\theta I_1(k\sin\theta)\\
&\quad+\begin{bmatrix}T^3_n\\T^4_n\end{bmatrix}\sin^2\theta I_0(k\sin\theta)\Big]+\cos(k\cos\theta)\Big[\begin{bmatrix}T^1_n\\T^2_n\end{bmatrix}k\cos\theta I_0(k\sin\theta)\\
&\quad+\begin{bmatrix}T^3_n\\T^4_n\end{bmatrix}(2\cos\theta I_0(k\sin\theta)+k\sin\theta\cos\theta I_1(k\sin\theta))\Big]\Big\},\\
\begin{bmatrix}S^5_n\\S^6_n\end{bmatrix}&=\begin{bmatrix}(1-n)\\(3-n)\end{bmatrix}\frac{C_n^{-\frac{1}{2}}(\cos\theta)}{\sin\theta}+\int_0^\infty dk\Big\{k\cos\theta\sin(k\cos\theta)\Big[-\begin{bmatrix}T^1_n\\T^2_n\end{bmatrix}I_1(k\sin\theta)\\
&\quad-\begin{bmatrix}T^3_n\\T^4_n\end{bmatrix}\sin\theta I_0(k\sin\theta)\Big]+\sin\theta\cos(k\cos\theta)\Big[\begin{bmatrix}T^1_n\\T^2_n\end{bmatrix}kI_0(k\sin\theta)\\
&\quad+\begin{bmatrix}T^3_n\\T^4_n\end{bmatrix}(2I_0(k\sin\theta)+k\sin\theta I_1(k\sin\theta))\Big]\Big\},\\
\begin{bmatrix}S^7_n\\S^8_n\end{bmatrix}&=-\begin{bmatrix}(n^2-1)\\(3-n)(1-n)\end{bmatrix}\frac{C_n^{-\frac{1}{2}}(\cos\theta)}{\sin\theta}+\begin{bmatrix}S^5_n\\S^6_n\end{bmatrix}-\int_0^\infty dk\Big\{k\cos(k\cos\theta)\\
&\quad\times\Big[-k\cos^2\theta\Big(\begin{bmatrix}T^1_n\\T^2_n\end{bmatrix}I_1(k\sin\theta)+\begin{bmatrix}T^3_n\\T^4_n\end{bmatrix}\sin\theta I_0(k\sin\theta)\Big)\\
&\quad+\sin^2\theta\Big(\begin{bmatrix}T^1_n\\T^2_n\end{bmatrix}kI_1(k\sin\theta)+\begin{bmatrix}T^3_n\\T^4_n\end{bmatrix}(2I_1(k\sin\theta)+k\sin\theta I_0(k\sin\theta)\Big)\Big]\\
&\quad-k\cos\theta\sin(k\cos\theta)\Big[\begin{bmatrix}T^1_n\\T^2_n\end{bmatrix}(2k\sin\theta I_0(k\sin\theta)-I_1(k\sin\theta))\\
&\quad+\begin{bmatrix}T^3_n\\T^4_n\end{bmatrix}(3\sin\theta I_0(k\sin\theta)+2\sin^2\theta kI_1(k\sin\theta))\Big]\Big\}.
\end{aligned} \tag{A 12}$$

A.3. *Collocation equations for the first order*

Satisfying (2.26) and (2.30*b*, *c*) at p distinct points on the first quadrant of the sphere results in the following $3p$ equations:

$$-U_{(1)}\cos\theta_i = \sum_{n-2}^{2p} [E^{(2)}_{n(1)} S^3_n(1,\theta_i) + F^{(2)}_{n(1)} S^4_n(1,\theta_i), \tag{A 13}$$

$$-U_{(1)}\sin\theta_i = \sum_{n-2}^{2p} [E^{(2)}_{n(1)} S^5_n(1,\theta_i) + F^{(2)}_{n(1)} S^6_n(1,\theta_i) + \frac{2}{\sin\theta_i} E^{(1)}_{n(1)} C_n^{-\frac{1}{2}}(\cos\theta_i)], \tag{A 14}$$

$$\begin{aligned} &-U_{(1)}\sin\theta_i - \phi\frac{\partial}{\partial\theta}\left\{\frac{1}{\sin\theta}\frac{\partial}{\partial\theta}\sin\theta - V\sin\theta\left[1-\left(\frac{\sin\theta}{b}\right)^2\right] + \sin\theta\right. \\ &\left. + \sum_{n=2}^{2m} [E^{(2)}_{n(0)} S^5_n(1,\theta) + F^{(2)}_{n(0)} S^6_n(1,\theta)]\right\}_{\theta=\theta_i} \\ &= \sum_{n-2}^{2p}\left[E^{(2)}_{n(1)} S^7_n(1,\theta) + F^{(2)}_{n(1)} S^8_n(1,\theta_i) - \frac{2(2n-1)\kappa}{\sin\theta_i} E^{(1)}_{n(1)} C_n^{-\frac{1}{2}}(\cos\theta_i)\right], \end{aligned} \tag{A 15}$$

where $2p$ is the order of the first-order field. Again, the above equations are valid for Poiseuille flow. Those valid for uniform flow may be obtained by setting $V = 0$ in (A 15).

REFERENCES

Bleys, G. & Joos, P. 1985 Adsorption kinetics of bolaform surfactants at the air/water interface. *J. Phys. Chem.* **89**, 1027–1032.

Brenner, H. 1970 Pressure drop due to the motion of neutrally buoyant particles in duct flows. *J. Fluid Mech.* **43**, 641–660.

Brenner, H. 1971 Pressure drop due to the motion of neutrally buoyant particles in duct flows. II. Spherical droplets and bubbles. *Indust. Engng Chem. Fundam.* **10**, 537–543.

Bretherton, F. 1961 The motion of long bubbles in tubes. *J. Fluid Mech.* **10**, 166–188.

Davis, R. E. & Acrivos, A. 1966 The influence of surfactants on the creeping motion of bubbles. *Chem. Engng Sci.* **21**, 681–685.

Frumkin, A. & Levich, V. 1947 *Zh. Fiz. Khim.* **21**, 1183.

Ginley, G. M. & Radke, C. J. 1989 The influence of soluble surfactants on the flow of a long bubble through a cylindrical capillary. *Am. Chem. Soc. Symp. Series* **396**, 480–501.

Goldsmith, H. & Mason, S. 1963 The flow of suspensions through tubes. II. Single large bubbles. *J. Colloid Interface Sci.* **35**, 183–199.

Haberman, W. L. & Sayre, R. M. 1958 Motion of rigid and fluid spheres in stationary and moving liquids inside cylindrical tubes. *David W. Taylor Model Basin Rep.* 1143. US Navy Dept.

Happel, J. & Brenner, H. 1973 *Low Reynolds Number Hydrodynamics*, 2nd edn. Noordhoff.

Harper, J. F. 1973 On bubbles with small immobile adsorbed films rising in liquids at low Reynolds numbers. *J. Fluid Mech.* **58**, 539–545.

Harper, J. F. 1982 Surface activity and bubble motion. *Appl. Sci. Res.* **38**, 343–351.

He, Z., Dagan, Z. & Maldarelli, C. 1990 The influence of surfactant on the motion of a fluid sphere in a tube. Part 2. The stagnant cap regime. *J. Fluid Mech.* (submitted).

Herbolzheimer, E. 1987 The effect of surfactant on the motion of a bubble in a capillary. *AIChE Annual Meeting, Nov. 15–20, NY, Paper* 68j.

Hirasaki, G. J. & Lawson, J. B. 1985 Mechanisms of foam flow in porous media: Apparent viscosity in smooth capillaries. *Soc. Petrol. Engrs J.* **25**, 176–190.

Holbrook, J. A. & Levan, M. D. 1983*a* Retardation of droplet motions by surfactant. Part 1 Theoretical development and asymptotic solutions. *Chem. Engng Commun.* **20**, 191–207.

HOLBROOK, J. A. & LEVAN, M. D. 1983*b* Retardation of droplet motion by surfactant. Part 2 Numerical solutions for exterior diffusion, surface diffusion, and adsorption kinetics. *Chem. Engng Commun.* **20**, 273–290.

HOMMELEN, J. R. 1959 The elimination of errors due to evaporation of the solute in the determination of surface forces. *J. Colloid Sci.* **14**, 385–400.

HYMAN, W. A. & SKALAK, R. 1969 *Tech. Rep.* 3, Proj. No. NR 062-393, Dept. Civil Engng and Engng Mech., Columbia University.

HYMAN, W. A. & SKALAK, R. 1970 *Tech. Rep.* 5, Proj. No. NR 062-393, Dept. Civil Engng and Engng Mech., Columbia University.

JOOS, P. & SERRIEN, G. 1989 Adsorption kinetics of lower alkanols at the air-water interface: Effect of structure makers and structure breakers. **127**, 97–103.

LEICHTBERG, S., PFEFFER, R. & WAINBAUM, S. 1976 Stokes flow past finite coaxial clusters of spheres in a circular cylinder. *Intl J. Multiphase Flow* **3**, 147–169.

LEVAN, M. D. & NEWMAN, J. 1976 The effect of surfactant on the terminal and interfacial velocities of a bubble or drop. *AIChE J.* **22**, 695.

LEVAN, M. D. & HOLBROOK, J. 1989 Motion of a droplet containing surfactant. *J. Colloid Interface Sci.* **131**, 242–251.

LEVICH, V. G. 1962 *Physicochemical Hydrodynamics.* Prentice-Hall.

MARTINEZ, M. & UDELL, K. 1989 Boundary integral analysis of the creeping flow of long bubbles in capillaries. *Trans. ASME* E: *J. Appl. Mech.* **56**, 211–217.

MARTINEZ, M. & UDELL, K. 1990 Axisymmetric creeping motion of drops through circular tubes. *J. Fluid Mech.* **210**, 565–591.

MOULAI-MOSTEFA, N., MEISTER, E. & BARTHES-BIESEL, D. 1986 Effect of surfactant on the flow of large gas bubbles in capillary tubes. *Physicochemical Hydrodynamics: Interfacial Phenomena. NATO conference, LaRabida, Espagne, July 11–15, 1986.*

NEWMAN, J. 1967 Retardation of falling drops. *Chem. Engng Sci.* **22**, 83–85.

PARK, C.-W. & HOMSY, G. M. 1984 Two phase displacement in Hele-Shaw cells: theory. *J. Fluid Mech.* **139**, 291–308.

PROBSTEIN, R. 1989 *Physicochemical Hydrodynamics: An Introduction*, pp. 308–311. Butterworths.

RATULOWSKI, J. & CHANG, H.-C. 1990 Marangoni effects of trace impurities on the motion of long gas bubbles in capillaries. *J. Fluid Mech.* **210**, 303–328.

REINELT, D. & SAFFMAN, P. 1985 The penetration of a finger into a viscous liquid in a channel and tube. *SIAM J. Sci. Statist. Comput.* **6**, 542–561.

SADHAL, S. S. & JOHNSON, R. E. 1982 Stokes flow past bubbles and drops partially coated with thin films. Part 1. Stagnant cap of surfactant film – exact solution. *J. Fluid Mech.* **126**, 237–250.

SAVIC, P. 1953 Circulation and distortion of liquid drops falling through a viscous medium. *Nat. Res. Counc. Can., Div. Mech. Engng Rep.* MT-22.

SAVILLE, D. A. 1973 The effects of interfacial tension gradients and droplet behavior. *Chem. Engng J.* **5**, 251–259.

SCHECHTER, R. S. & FARLEY, R. W. 1963 Interfacial tension gradients and droplet behavior. *Can. J. Chem. Engng* **41**, 103.

SHEN, E. I. & UDELL, K. S. 1985 A finite element study of low Reynolds number two phase flow in cylindrical tubes. *Trans. ASME* E: *J. Appl. Mech.* **52**, 253–256.

WANG, H. & SKALAK, R. 1969 Viscous flow in a cylindrical tube containing a line of spherical particles. *J. Fluid Mech.* **38**, 75–96.

WASSERMAN, M. L. & SLATTERY, J. C. 1969 Creeping flow past a fluid globule when a trace of surfactant is present. *AIChE J.* **15**, 533–548.

WESTBORG, H. & HASSAGER, O. 1989 Creeping motion of long bubbles and drops in capillary tubes. *J. Colloid Interface Sci.* **133**, 135–147.